

The PDS starburst galaxies

Roger Coziol^{1,2}, Carlos A. O. Torres¹, Germano R. Quast¹, Thierry Contini³

and

Emmanuel Davoust⁴

Received _____; accepted _____

¹Laboratório Nacional de Astrofísica - LNA/CNPq, CP 21, 37500-000 Itajubá, MG, Brazil

²Present address: Observatório Nacional, CEP 20921-400, Rio de Janeiro, Brasil

³School of Physics & Astronomy, Tel Aviv University, 69978 Tel Aviv, Israel

⁴Observatoire Midi-Pyrénées, UMR 5572, F-31400 Toulouse, France

ABSTRACT

We discuss the nature of the galaxies found in the Pico dos Dias Survey (PDS) for young stellar objects. The PDS galaxies were selected from the IRAS Point Source catalog. They have flux density of moderate or high quality at 12, 25 and 60 μm and spectral indices in the ranges $-3.00 \leq \alpha(25, 12) \leq +0.35$ and $-2.50 \leq \alpha(60, 25) \leq +0.85$. These criteria allowed the detection of 382 galaxies, which are a mixture of starburst and Seyfert galaxies. Most of the PDS Seyferts are included in the catalog of warm IRAS sources by de Grijp et al. (1987). The remaining galaxies constitute a homogeneous sample of luminous ($\log(L_{\text{B}}/L_{\odot}) = 9.9 \pm 0.4$) starburst galaxies, 67% of which were not recognized as such before.

The starburst nature of the PDS galaxies is established by comparing their $L_{\text{IR}}/L_{\text{B}}$ ratios and IRAS colors with a sample of emission line galaxies from the literature already classified as starburst galaxies. The starburst galaxies show an excess of FIR luminosity and their IRAS colors are significantly different from those of Seyfert galaxies – 99% of the starburst galaxies in our sample have a spectral index $\alpha(60, 25) < -1.9$. As opposed to Seyfert galaxies, very few PDS starbursts are detected in X-rays.

In the infrared, the starburst galaxies form a continuous sequence with normal galaxies. But they generally can be distinguished from normal galaxies by their spectral index $\alpha(60, 25) > -2.5$. This color cut-off also marks a change in the dominant morphologies of the galaxies: the normal IRAS galaxies are preferentially late-type spirals (Sb and later), while the starbursts are more numerous among early-type spirals (earlier than Sbc). This preference of starbursts for early-type spirals is not new, but a trait of the massive Starburst Nucleus Galaxies (Coziol et al. 1997a). Like in other SBNG samples, the PDS starbursts show no preference for barred galaxies.

No difference is found between the starbursts detected in the FIR and those detected on the basis of UV excess. The PDS starburst galaxies represent the FIR luminous branch of the UV-bright starburst nucleus galaxies, with mean FIR luminosity $\log(L_{\text{IR}}/L_{\odot}) = 10.3 \pm 0.5$ and redshifts smaller than 0.1. They form a complete sample limited in flux in the FIR at 2×10^{-10} $\text{erg cm}^{-2} \text{ s}^{-1}$.

Subject headings: surveys – galaxies: starburst – galaxies: Seyfert – infrared: galaxies – X-rays: galaxies

1. Introduction

Since their discovery a few decades ago, starburst galaxies have been a constantly growing field of research. This increasing interest is due to the fact that what was once considered as a peculiar phenomenon affecting only a small fraction of the local population of galaxies turns out to be of a more general nature, involving mechanisms by which galaxies form and evolve (Larson 1990; Kennicutt 1990; van den Bergh et al. 1996; Coziol et al. 1997b, 1998; Driver et al. 1998). Yet, our present knowledge on the properties of starburst galaxies rests on the analyses of a rather limited number of data sets and fundamental questions on their nature still remain to be answered. For example, is there a relation between the small-mass and metal poor H II galaxies and the more massive and chemically evolved Starburst Nucleus Galaxies (SBNGs)? What is the difference between starburst galaxies which are UV-bright and those which are selected based on a strong emission in the far infrared (FIR)? Is there a relation between Active Galactic Nuclei (AGN) and starburst activity? Are all starbursts efficient X-rays emitters? What is the dominant morphology of starburst galaxies?

In this context, we have judged useful to present this new homogeneous sample of relatively nearby and luminous starburst galaxies selected in the FIR: the PDS (which stands for Pico dos Dias Survey) starburst galaxies. The fact that starbursts are easily detected in the FIR is not surprising (Meadows et al. 1990; Allen et al. 1991; Contini et al. 1998). In their selected sample of IRAS galaxies, for example, Allen et al. (1991) found 90% starburst and 10% Seyfert galaxies. Similar ratios were found in the Contini et al. (1998) sample of Markarian UV-bright galaxies. In the Montreal Blue Galaxy (MBG) survey, 85% of the UV-bright starburst galaxies are also IRAS sources (Coziol et al. 1997a). Interestingly, the percentage of AGNs seems to increase with the FIR luminosity. In their sample of Luminous Infrared Galaxies (LIGs), Veilleux et al. (1995) found 41% Seyfert galaxies and 59% starbursts. For the PDS galaxies, the discovery ratios are 38% AGNs for 62% starbursts.

The organization of this paper is as follows. In section 2, we present the list of the PDS starburst galaxies. In section 3, the starburst nature of these galaxies is established by comparing their IRAS and optical characteristics with those of normal and starburst galaxies taken from the literature. The IRAS color-color diagrams of the PDS starbursts are compared to those of the AGNs and two criteria are proposed to distinguish between these two types of activity in galaxies. The application of these criteria allows us to identify 9 misclassified Seyfert galaxies. In section 4, some of the characteristics of the PDS starbursts are examined. A summary of our results is given in section 5.

2. The sample of PDS galaxies

The Pico dos Dias survey (PDS) is a systematic search performed at the Observatório do Pico dos Dias (OPD – operated by the Laboratório Nacional de Astrofísica (LNA), Conselho Nacional de Desenvolvimento Científico e Tecnológico (CNPq)) to discover young stellar objects from their FIR properties (Gregorio-Hetem et al. 1992; Torres et al. 1995). The candidates, selected from the IRAS Point Source Catalog (IPSC), have flux density qualities 2 or 3 at 12, 25 and 60 μm , and spectral indices in the ranges $-3.00 \leq \alpha(25, 12) \leq +0.35$ and $-2.50 \leq \alpha(60, 25) \leq +0.85$ (Torres & Quast 1995), where the spectral indices are defined as $\alpha(\lambda_1, \lambda_2) = \log(S_{\lambda_1}/S_{\lambda_2})/\log(\lambda_2/\lambda_1)$, and S_{λ_1} is the flux in Jansky at wavelength λ_1 . The appearance of all the young stellar candidates was examined on the Digitized Sky Survey plates and the galaxy-like objects were placed on a separate list, which we call the PDS galaxy list. Some star-like AGNs were also included in this list after establishing their nature from the Véron–Cetty & Véron (1996) compilation. The goal of the present paper is to determine the nature of all the objects in the PDS galaxy list.

Initially, the PDS galaxies were composed of 388 objects. An entry for all these sources was found in NED⁵. Two objects turned out to be planetary nebulae and 3 others were identified with H II regions in M33 and M101. The luminous quasar 3C 273 was also detected. After removing these 6 objects, we were left with 382 galaxies.

There are 122 AGNs in our list, distributed among 4 LINERs, 76 Seyfert 2 (Sy2) and 42 Seyfert 1 (Sy1). The fact that there are so few LINERs is intriguing, considering the high volume density of these objects in the nearby Universe ($\sim 30\%$ of the local luminous galaxies; Heckman 1980; Ho, Filippenko & Sargent 1997). We note that 84% of the PDS AGNs are included in the warm IRAS source catalog of de Grijp et al. (1987); this suggests that they used similar selection criteria in the FIR as ours. Because de Grijp et al. were only interested in AGNs, they applied an arbitrary cut-off to the color $\alpha(60,25)$ to separate them from normal galaxies. In the PDS, the limit applied to this color is slightly below this cut-off, allowing the inclusion of numerous non-AGN galaxies. However, we will show that these galaxies are not normal but mostly starbursts.

The 260 PDS non-AGN galaxies in our list are either already known starburst galaxies (33%) or unclassified galaxies that we consider to be starbursts. It is noteworthy that 67% of the PDS starburst

⁵The NASA/IPAC Extragalactic Database.

galaxies were not recognized as such before.

To facilitate our analysis, we retained only the galaxies which have fluxes with high or intermediate qualities in the IRAS Faint Source Catalog (IFSC). We rejected 14 galaxies of low quality flux and 46 others because they have a Galactic latitude $|b| < 10^\circ$, and consequently do not appear in the IFSC. 200 galaxies were thus left in our sample.

In Table 1 we present the 200 PDS starburst candidates. Column 1 gives their IRAS name. A capital X at the end of the name identifies the galaxy as an X-ray source, according to the ROSAT catalog (Voges et al. 1996). Column 2 gives another acronym from NED. Other properties also taken from NED are: the 1950 coordinates of the galaxy (columns 3 and 4), the redshift (column 4), the B magnitude (column 6) and the morphology (column 7). We note that our list contains two of the most famous starbursts: M82 and NGC 7714.

In Table 2, we give the optical and FIR characteristics of our sample of galaxies. Columns 2 and 3 correspond to the absolute magnitude and B luminosity, which were determined using the magnitudes quoted in Table 1 and assuming $H_0 = 75 \text{ km s}^{-1} \text{ Mpc}^{-1}$. No correction for Galactic reddening was applied. The infrared luminosity in column 4 was determined from the relation: $\log(L_{\text{IR}}) = \log(F_{\text{IR}}) + 2 \log[z(z+1)] + 57.28$, where z is the redshift and $F_{\text{IR}} = 1.26 \times 10^{-11}(2.58S_{60} + S_{100}) \text{ erg cm}^{-2} \text{ s}^{-1}$ (Lonsdale et al. 1985). The mean FIR luminosity of the PDS starbursts is $2 \times 10^{10} L_\odot$, slightly less than the mean luminosity of the LIGs studied by Veilleux et al. (1995). In columns 5, 6, and 7 we give the IRAS spectral indices. In general, the differences between the spectral indices determined using the IFSC or IPSC fluxes are marginal. The quality indices in the four IRAS bands are given in column 8.

An interesting characteristic of our sample is the different fractions of galaxies with different activity types detected in X-rays: 2 of the 4 LINERs (50%) were detected, as compared to 71% of the Sy1, 22% of the Sy2 and only 4% of the starbursts. These differences between the starbursts and the two Seyfert galaxies are highly significant considering that in our sample the Sy2 are almost twice as numerous as the Sy1 and the starbursts still more numerous than the Sy2.

3. The starburst nature of the PDS galaxies

We define a starburst galaxy as an emission-line galaxy where the source of ionization of the gas is of stellar origin, as determined from standard emission line ratio diagnostic diagrams (Baldwin, Phillips &

Terlevich 1981; Veilleux & Osterbrock 1987). This first criterion eliminates the Seyfert galaxies, but also the LINERs whose source of ionization is not clearly defined. The starburst galaxies have $H\alpha$ luminosities from 10^{39} up to a few 10^{42} erg s^{-1} (Balzano 1983; Coziol 1996), implying unusually high present star formation rates. Obviously, these galaxies cannot sustain such elevated star formation rates for a very long time (hence the name starburst; Weedman et al. 1981), unless they are replenished in gas, following some kind of interaction with another galaxy or with its environment (Huchra 1977; Taylor et al. 1996), or if the star formation is regulated by internal processes, probably related to supernovae feedback (Searle & Sargent 1972; Gerola, Seiden & Schulman, 1980; Krügel & Tutukov 1993). From the University of Michigan (UM) survey, Salzer et al. (1989) have shown that the starbursts present a variety of types related to their morphologies. Based on similar characteristics, we can regroup these types in two broad categories (Coziol et al. 1994): the H II galaxies which are small mass and metal poor galaxies and the Starburst Nucleus Galaxies (SBNGs) which are more massive and chemically evolved.

Starburst galaxies are usually detected by the presence of emission-lines in their spectra (using the objective-prism technique) or by a UV color excess (using the multiple filters technique). The two methods yield similar results (Coziol et al. 1993), the only difference being that objective-prism surveys are biased against SBNGs while multiple colors surveys are biased against H II galaxies (Coziol 1996). Starburst galaxies detected in the FIR are generally similar to the SBNGs detected in the optical (Allen et al. 1991; Veilleux et al. 1995). However, at the extreme end of the FIR range one finds a new type of starburst galaxy: the ultra Luminous Infrared Galaxies (uLIGs), which emit most of their energy in the FIR (Sanders et al. 1988). One important property distinguishes the uLIGs from the other two types of starbursts: while all the uLIGs are cases of massive galaxies in interaction (Mirabel & Duc 1993), only a small fraction ($\sim 1/4$) of the SBNGs and H II galaxies clearly are (Telles & Terlevich 1995; Coziol et al. 1997).

In what follows, we determine the starburst nature of the galaxies in our sample from their FIR luminosity and color. Our method is semi-empirical in nature. We use simple models to interpret the $L_{\text{IR}}/L_{\text{B}}$ ratios (Coziol et al. 1996) and IRAS colors (Sekiguchi 1987) of the galaxies and compare the characteristics of the PDS galaxies with those of different samples of normal and starburst galaxies taken from the literature. The sample of normal galaxies is composed of galaxies from the list of Stauffer (1982), Kennicutt (1983) and Hogg et al. (1993), from which we eliminated, using their identification in NED, all the known Seyferts, interacting, UV-bright and starburst galaxies (such as UM, Arp, Markarian, Kiso, MBG or Zwicky-like galaxies). The sample of starburst galaxies is composed of three samples representing the different types of starbursts: (a) SBNGs from the UM survey (Salzer et al. 1989), the Balzano’s sample

of Markarian galaxies (1983) and the MBG survey (Coziol et al. 1993, 1994, 1997a, 1997b); (b) H II galaxies from the catalog of Terlevich et al. (1991) and from the Calan–Tololo survey (Peña et al. 1991); (c) Luminous Infrared Galaxies (LIGs), as observed by Veilleux et al. (1995), which most luminous members are similar to the uLIGs.

3.1. The FIR luminosity excess in starbursts

In Figure 1, we present the diagram of L_{IR} as a function of L_{B} . Coziol (1996) showed that starburst galaxies present a typical excess of FIR luminosity as compared to normal spiral galaxies. In Figure 1a, this phenomenon is illustrated by comparing the luminosities of the PDS starbursts with the mean values found for different samples of galaxies, as determined in Coziol (1996). For comparison purposes, we distinguished between early-type (earlier than Sbc) and late-type galaxies (Sbc and later). It can be seen that most of the PDS galaxies show a ratio $L_{\text{IR}}/L_{\text{B}}$ higher than 1, similar to the SBNGs.

In Figure 1b, which concerns the PDS Seyfert galaxies, we also show the mean values found by Roberts & Haynes (1994) for normal galaxies with different morphologies. This sample is probably more representative of normal galaxies than the samples of Stauffer, Hogg et al. or Kennicutt, because it is not biased towards emission-line galaxies. Comparing the PDS galaxies (starbursts and AGNs) with the normal galaxies, it can be seen that the former have normal blue luminosities. Like the SBNGs, their mean absolute B magnitude $M_{\text{B}} = -20.0 \pm 1.0$ suggests that they generally are massive galaxies. This result is consistent with the fact that small-mass starburst galaxies (like the H II galaxies for example) are generally deficient in dust (Coziol 1996).

Although the FIR-luminosity-excess criterion enables one to distinguish starbursts from normal galaxies, it does not allow to separate them from AGNs. Indeed, in Figure 1b we see that, in general, the Seyfert galaxies show $L_{\text{IR}}/L_{\text{B}}$ ratios comparable to those of SBNGs. This is a characteristic of Seyfert galaxies (Coziol 1996). The nature of the FIR excess in these galaxies is ambiguous, because the contribution of the active nucleus to the FIR luminosity is not well determined. If this contribution were negligible, then the excess of FIR luminosity would imply high star forming rates.

3.2. A model for the typical FIR colors of galaxies

In Figure 2a, we show the diagram of the spectral indices $\alpha(60,25)$ versus $\alpha(100,60)$ for the sample of normal galaxies, as defined above. It can be seen that normal galaxies occupy only a small region of this diagram. There also seems to be no difference in colors between the normal early-type galaxies and the late-types ones (see Sauvage & Thuan 1994 for a discussion of this phenomenon in normal galaxies).

In Figure 2b, the same diagram is shown for the samples of starburst galaxies. The FIR colors of the starbursts are clearly offset from those of normal galaxies, but a significant region of overlap exists. This result reminds one of the observation made by Huchra (1977) about the Markarian galaxies, namely that starbursts are not a new class of objects but rather a subset of normal galaxies. This seems to be true in the FIR as well.

To interpret the data, we use a two-blackbody model composed of a cirrus-like, cold component with a temperature $\sim 27\text{K}$, added to a hot component, associated with a burst of star formation (Sekiguchi 1987). In Figure 2, the temperature of the hot component varies from 60K to 100K. The numbers on the grid indicate the fractional contribution of the hot component to the total FIR luminosity. For the sample of normal galaxies, the contribution of the hot component varies between 0.6 and 0.9 and the temperature varies between 65K and 80K. In the starbursts, the contribution from the hot component is generally higher than 0.8 and the temperature is almost always higher than 70K. The interpretation of this difference is straightforward (Sekiguchi 1987; Coziol 1996): the higher star formation rates in starburst galaxies simply increases the quantity of hot dust.

It is instructive to study the location of the various types of starbursts in Figure 2b. The small dispersion for the colors of the SBNGs, for example, suggests similar characteristics for the bursts (similar intensities, ages or dust contents). The larger dispersion for the LIGs, on the other hand, suggests a more heterogeneous group. This difference between the two types of starbursts may be explained in part by different levels of extinction, which is generally higher in the LIGs than in the optically selected SBNGs (Veilleux et al. 1995). In Figure 2b for instance, some LIGs have colors similar to a pure blackbody. In these galaxies most of the light may be absorbed by dust and reemitted in the FIR. The fact, on the other hand, that many UV-bright SBNGs are also FIR emitters suggests that the dust distribution in these galaxies is rather patchy (Calzetti et al. 1996).

On average, the LIGs show a higher hot-component contribution and/or a higher dust temperature than the SBNGs. The LIGs, therefore, may have higher star formation rates or younger bursts than the

SBNGs (Coziol 1996). But, some may also hide an AGN (Sanders et al. 1988).

For the H II galaxies, the high dust temperatures suggested by the model are probably better explained by their low metallicities and young ages. A young starburst contains a larger number of massive stars than a more evolved one, and a metal-poor ionized gas reaches higher temperatures than a metal-rich one.

3.3. Discrimination between normal, starburst and Seyfert galaxies using FIR colors

In Figure 3a, we now apply our model to the PDS starburst galaxies. We deduce that the PDS starburst galaxies have IRAS colors which are typical of SBNGs. This conclusion is consistent with our previous classification based on the ratio $L_{\text{IR}}/L_{\text{B}}$.

In Figure 3a, we distinguish between the PDS starbursts detected in the UV, the galaxies assumed to be in interaction (the Arp galaxies) and the pure IRAS galaxies (that is, the FIR galaxies with no other special known characteristics). In general, the colors of the three types of galaxies are similar. Therefore, whatever the origin of the bursts in these galaxies, the result in terms of colors seems to be the same.

In order to test how arbitrary our criteria for selecting starbursts in the FIR are, we have examined the nature of the galaxies which have a IPSC color $\alpha(60, 25) < -2.5$. This specific criterion was tested, because we noticed that it eliminates a good number of IRAS galaxies in the IPSC. Using NED, we identified a new sample of 210 IRAS galaxies with a IPSC color $\alpha(60, 25) < -2.5$. Among these galaxies only 23 (11%) were recognized as Seyfert galaxies. We call the remaining 187 galaxies the IRAS normal galaxies. Indeed, in Figure 2a, we can see that the IRAS normal galaxies have colors typical of normal galaxies.

In Table 3, the mean B and FIR luminosities and dispersions for the IRAS normal galaxies are compared to those of the PDS starburst and Seyfert galaxies. All these galaxies have comparable luminosities. In column 4 of Table 3, we also give the $L_{\text{IR}}/L_{\text{B}}$ ratios observed in all these galaxies. The IRAS normal galaxies do not show the same excess of FIR luminosity as the PDS starbursts. A Kolmogorov–Smirnov test allows one to reject, at a level of confidence higher than 99.9%, the hypothesis that the two distributions were taken from the same population. Therefore, without completely separating them from normal galaxies our color criteria allow us to effectively select starburst galaxies.

In Figure 3b, we present the color-color diagram $\alpha(60,25)$ vs. $\alpha(100,60)$ for the PDS Seyfert galaxies. As already noted by de Grijp et al. (1987), the FIR spectral indices of Seyfert galaxies are generally flatter than those of starbursts. Only a small fraction of the PDS Seyfert galaxies in Figure 3b have FIR colors

similar to those of the starbursts. There seems to be more Sy2 than Sy1 in this situation: about 38% of the Sy2 compared to only 10% of the Sy1. Above the cut-off defined by de Grijp et al. ($\alpha(60,25) > -1.5$) the Sy2 show a slightly flatter $\alpha(100,60)$ spectral index than the Sy1. In Table 3, we also see that the Sy2 show a similar mean excess of FIR luminosity to that of the starbursts, while this ratio for the Sy1 is normal. Comparing them with the IRAS normal galaxies, a Kolmogorov–Smirnov test allows to reject, but only at the 92% confidence level, the hypothesis that the Sy2 distributions comes from the same population as the normal ones. The same hypothesis simply cannot be rejected for the Sy1.

The differences in FIR characteristics among the various types of galaxies are better observed in the diagrams $\alpha(60,25)$ vs. $\alpha(25,12)$, presented in Figure 4. In Figure 4a, most of the PDS starbursts have a color $\alpha(60,25)$ between -1.9 and -2.5 . In Figure 4b, the PDS Sy2 with a color $\alpha(60,25)$ higher than -1.9 have a color $\alpha(25,12)$ lower than -1.5 , while it is the contrary for the Sy1. This last cut-off also seems to separate most of the X-ray AGNs from the non X-ray ones. But it is the contrary for the starbursts.

In Figure 4b, we have also placed the IRAS normal galaxies. As can be seen, the FIR color distribution of the normal galaxies merges with those of the starburst galaxies. In reality, all these galaxies form a continuous sequence in colors. We distinguished the starbursts based on the color criterion⁶ $\alpha(60,25) > -2.5$. In section 4, we will show that this color cut-off also marks a change in the dominant morphological types of the galaxies.

3.4. Spectroscopic observations of misclassified AGNs

In Figure 4a, 17 of the PDS starbursts show a spectral index $\alpha(60,25) > -1.9$. Considering the large difference between the rest of the starbursts and the AGNs in this diagram, we wondered if these 17 starbursts could not be misidentified AGNs. Likewise, the fact that many more PDS AGNs than starbursts are detected in X-rays (only 11 PDS starbursts are X-ray sources) also suggests that some of these starbursts are misidentified AGNs. To verify the nature of these galaxies, spectroscopic observations were obtained for 12 of the 17 starbursts with $\alpha(60,25) > -1.9$ and 3 X-ray starbursts. In August 1997, 2 galaxies (IC2202 and IRAS14454-4343) were observed with the 1.6m telescope at the OPD and 2 others (IIZw083 and IRAS19265-4338) were observed at the 1.52m telescope at ESO. The remaining starbursts were observed in January and March 1998 with the 1m WISE telescope in Israel.

⁶Note that it is the spectral index as determined using the IFSC fluxes that we now use.

At the OPD, a Boller & Chivens spectrograph was used in conjunction with a 1024×1024 , SIT, back-illuminated CCD. Two spectra with resolution $\sim 2 \text{ \AA}$ were taken using a 600l/mm grating centered alternatively at 4600 and 6300 \AA . The slit had a width of ~ 2.5 arsec and was aligned in position E–W across the center of the galaxies. At the 1.52m of ESO, the data were acquired with a Boller & Chivens spectrograph and a 2048×2048 Loral, UV flooded CCD. The grating used had a dispersion of 187 $\text{\AA}/\text{mm}$ providing a spectral coverage of $\sim 3000 - 9000 \text{ \AA}$ and a resolution of about 10 \AA . The slit width covered ~ 3 arsec of the center of the galaxies and was positioned close to the parallactic angle. At the 1m telescope of the Wise Observatory (Israel) a FOSC spectrograph was used with a 1024×1024 Tektronics CCD. The spectral coverage was $\sim 3500 - 7300 \text{ \AA}$ and the resolution was about 8 \AA . The slit width covered ~ 5 arsec of the center of the galaxies and was also positioned close to the parallactic angle. All the spectra were reduced according to standard procedures under IRAF. These include bias subtraction, flat-field and distortion corrections, cosmic ray removal, sky subtraction, wavelength and flux calibrations.

Table 4 gives the ratios of the most prominent emission lines which we used to classify the activity types of the galaxies. Although some of these galaxies have very strong emission lines, they do not seem to have broad components typical of Sy1 galaxies. Figure 5 shows one of the diagnostic diagrams which we used for our classification. The results are reported in column 7 of Table 4. Note that the same classification is obtained using other line ratios. As we suspected, 9 of the 12 PDS starbursts with $\alpha(60,25) > -1.9$ (identified by crosses in Figure 4a) are misidentified AGNs (Sy2 or LINER). The three remaining starburst galaxies have color values at the borderline between those of starbursts and AGNs (in Figure 4a, they are identified by a square and occupy the extreme positions at the top of the sequence traced by the starbursts). The color difference between the AGNs and the starbursts, in Figure 4a, seems remarkably well established since 99% of the PDS starbursts have a spectral index $\alpha(60,25) > -1.9$.

Following our spectral classification, the starburst nature of the 3 X-ray galaxies classified as starbursts on the basis of their colors is confirmed, although NGC 3310 could also be a LINER. The case of NGC 3690 is complicated by the fact that this is really two interacting galaxies. It is not clear, therefore, what is the origin of the X-ray emission in this system. It could come from hot gas between the two interacting galaxies or be related only to one of the galaxies. Again we note that the western galaxy of this pair shows line ratios at the borderline separating starbursts from LINERs. As a common characteristic, the 4 X-ray starbursts have slightly higher excitation levels than normal SBNGs. All these galaxies could be of intermediate nature between AGN and starburst (Véron et al. 1997).

4. Properties of the PDS starbursts

In Figure 1, we have verified that the PDS galaxies are preferentially massive galaxies. This result is consistent with the observation that small-mass starburst galaxies are usually deficient in dust. In the H II galaxies the dust could have been easily ejected into the intergalactic medium (with a good part of the metals) by strong starburst winds. Alternatively, these galaxies may also be too young and have not had enough time to produce a sufficient amount of dust to be visible in the FIR. Being massive, the PDS galaxies are more similar to SBNGs. In this section, we will therefore continue our discussion by comparing some of the characteristics of the PDS starburst galaxies with those of the SBNGs.

In Figure 6, we present the morphologies of the PDS starbursts compared to those of the Markarian galaxies and the SBNGs of Balzano (1983). We can see that the distribution of the morphologies of the PDS galaxies is intermediate between those of these two samples. In particular, the PDS galaxies seem to contain a relatively high number of early-type spirals (Sb and earlier). This is a common trend of SBNG samples (Coziol et al. 1997a). In Figure 6, we verify that this trend in favor of early-type spirals is not observed in the sample of IRAS normal galaxies. In this case, the fraction of early-type galaxies falls drastically against that of the late-type ones.

We can also see in Figure 6 that the fraction of barred PDS starbursts is similar to that observed in other samples of SBNGs. This fraction is high, but not particularly so, if we judge from the high fraction of barred galaxies also observed in the IRAS normal galaxy sample. Like in other samples of SBNGs (Coziol et al. 1997a; Continni et al. 1998) the fraction of PDS galaxies with a bar seems to increase towards late-type galaxies. The PDS galaxies show no evidence to be preferably barred.

In Figure 7, we compare the FIR luminosities and the redshifts of the PDS galaxies with those of the UV-bright MBGs and IRAS galaxies selected by Allen et al. (1991). Coziol et al. (1997a) showed that the MBGs are the equivalent of the IRAS luminous galaxies at lower redshifts. The PDS starbursts, on the other hand, are observed in similar redshift ranges (from 0 to 0.1) as the MBGs. These two samples are limited to relatively low redshifts. The PDS galaxies are simply the FIR luminous equivalent of the nearby UV-bright SBNGs. The two diagonal lines in Figure 7 suggest that the PDS galaxies are flux limited in the FIR at 10^{-10} erg cm $^{-2}$ s $^{-1}$ and the MBGs at 10^{-11} erg cm $^{-2}$ s $^{-1}$.

5. Summary and conclusions

In this contribution, we have confirmed that starburst galaxies can be effectively detected and discriminated from normal galaxies and AGNs using criteria based on their FIR emission.

In comparison with normal galaxies, the starbursts typically show an excess of FIR luminosity and distinct colors. These differences are explained by a higher quantity of hot dust due to the higher star formation rates in starbursts as compared to normal galaxies. In the FIR, the starbursts form a continuous sequence with the normal galaxies, but can be distinguished based on a color $\alpha(60,25) < -2.5$. This color cut-off also marks a variation in the dominant morphological types of the galaxies: normal IRAS galaxies are mostly late-type (Sb and later) spirals, while starbursts are more numerous among the early-type ones (Sb and earlier). This result is consistent with the observations made by Devereux & Hameed (1997), and suggests that many early-type spiral galaxies are still actively forming stars. However, this preference of massive starburst for early-type morphologies is not new, but a trait of SBNGs (Coziol et al. 1997a).

Like for other samples of SBNGs, no preference for barred galaxies is found among the PDS starbursts. The role of the bar in starbursts is not well established. The fact that the number of barred starbursts increases towards the late-type morphologies may suggest that the bar is important only in the late-type starbursts. Alternatively, the bar could also have a shorter life time in a galaxy with a stronger bulge.

The PDS starbursts are mostly massive ($M_B = -20.0 \pm 1.0$). This result is consistent with the fact that the small-mass H II galaxies are relatively deficient in dust. In the H II galaxies the dust may have been swept away by starburst winds, or these galaxies may be too young to have produced enough dust. The FIR colors of the H II galaxies suggest that their dust temperatures are higher than those of the SBNGs. This phenomenon probably has something to do with the low metallicities of these galaxies, but also suggests a larger number of young stars than in the SBNGs and, consequently, younger age for the bursts in the H II galaxies than in the SBNGs.

In general, there seems to be no difference between the FIR characteristics of the UV-bright starbursts and those selected in the FIR. The PDS starbursts simply correspond to the FIR luminous branch of the UV-bright SBNGs with a mean FIR luminosity $\text{Log}(L_{\text{IR}}/L_{\odot}) = 10.3 \pm 0.5$ and redshift $z < 0.1$. The PDS starbursts, in particular, are limited in flux in the FIR at $10^{-10} \text{ erg cm}^{-2} \text{ s}^{-1}$ while the UV-bright starbursts are limited in flux at $10^{-11} \text{ erg cm}^{-2} \text{ s}^{-1}$.

Another interesting result of our analysis is the very few starbursts detected in X-rays. Only 4% of the

200 PDS starbursts were detected by ROSAT. Furthermore, the nature of 3 of these X-ray starbursts for which we obtained a spectrum was found to be ambiguous, the galaxies showing spectral characteristics intermediate between those of starbursts and LINERs. This result, and the fact that a very high number of Sy1 (71%), but few Sy2 (22%) were detected in X-rays, cautions against the utilization of the FIR, without other means of discrimination, to select starburst galaxies in order to study their X-ray properties. Our observations suggest, instead, that the contribution by starbursts to the cosmic X-ray background, for example, could be negligible (Hasinger 1998).

The relatively high fraction (38%) of AGNs in our sample is consistent with observations which suggest that the probability of finding an AGN increases with the FIR luminosity (de Grijp et al. 1987; Veilleux et al. 1995). In our sample, 62% of the AGNs are Sy2, 34% are Sy1 and the remaining 4% are LINERs. The higher number of Sy2 encountered is consistent with the idea that these galaxies are slightly richer in dust than the Sy1 (Malkan et al. 1998). The low fraction of LINERs, on the other hand, is consistent with the idea that these galaxies are low luminosity AGNs which are not in a starburst phase (Coziol 1996). Only 10% of the PDS Sy1 and 38% of the PDS Sy2 have a spectral index in the range $-2.5 \leq \alpha(60, 25) \leq -1.9$. But the most striking result of our analysis is the fact that only 1% of the PDS starbursts have a spectral index $\alpha(60, 25) > -1.9$. The few starbursts which passed this limit are at the extreme of the sequence traced by the starburst galaxies and show spectral characteristics at the borderline between those of starbursts and LINERs.

Our analysis clearly shows that Seyfert galaxies have distinct FIR colors from starburst galaxies. This means that the active nucleus in AGNs must contribute significantly to the FIR excess emission observed in these objects. Now, because this excess is, on average, barely equal to that observed in SBNGs, it suggests that the level of star formation in Seyfert galaxies may be different from that in starbursts. Taken at face value, our results imply that only a small fraction of the Seyfert galaxies, maybe $\sim 40\%$ of the Sy2 and $\sim 10\%$ of the Sy1, could be dominated by star formation. It is remarkable to find these fractions roughly consistent with those determined by González Delgado et al. (1997) based on their discovery of different star formation properties between Sy2 and Sy1 (for similar results see also Glass & Moorwood 1985; Maiolino et al. 1995; Hunt et al. 1997 and more recently Malkan et al. 1998). A better determination of the contribution of the active nucleus to the FIR is necessary in order to understand the relation of AGNs with starbursts.

The electronic version of the tables for the different samples of galaxies defined in this paper (including the 187 IRAS normal galaxies and the Seyfert galaxies) are available upon request to the first author.

We thank an anonymous referee for useful comments which allow us to improve the quality of our paper. R. C. acknowledges the CNPq for research fellowship. This research has made use of the NASA/IPAC Extragalactic Database (NED) which is operated by the Jet Propuls

REFERENCES

- Allen, D. A., Norris, R. P., Meadows, V. S., Roche, P. F. 1991, MNRAS, 248, 528
- Baldwin, J. A., Phillips, M. M., Terlevich, R. 1981, PASP, 93, 5
- Balzano, V. A. 1983, ApJ, 268, 602
- Calzetti, D., Kinney, A. L., Storchi-Bergmann, T. 1996, ApJ, 458, 132
- Contini, T., Considère, S., Davoust, E. 1998, A&AS, 130, 285
- Coziol, R. 1996, A&A, 309, 345
- Coziol, R., Contini, T., Davoust, E., Consière, S. 1998, in Abundance profiles: Diagnostic Tools for Galaxy History, D. Friedli, M.G. Edmunds, C. Robert, L. Drissen, eds., ASP conf series, in press (astro-ph/9802285)
- Coziol, R., Demers, S., Barnéoud, R., Peña, M. 1997a, AJ, 113, 1548
- Coziol, R., Contini, T., Davoust, E., Consière, S. 1997b, ApJ, 481, L67
- Coziol, R., Demers, S., Peña, M., Barnéoud 1994, AJ, 108, 405
- Coziol, R., Demers, S., Peña, M., Torres-Peimbert, S., Fontaine, G., Wesemael, F., Lamontagne, R., 1993, AJ, 105, 35
- Devereux, N. A., Hameed, S. 1997, AJ, 113, 599
- Driver, S. P., Fernández-Soto, A. Couch, W. J., Odewahn, S. C., Windhorst, R. A., Phillips, S., Lanzetta, K., Yahil, A. 1998, ApJ, 496, 93
- de Grijp, M. H. K., Miley, G. K., Lub, J. 1987, A&AS, 70, 95
- Gerola, H., Seiden, P. E., Schulman, L. S. 1980, ApJ, 242, 517
- González Delgado, R. M., Pérez, E., Tadhunter, C., Vilchez, M. J., Rodríguez-Espinosa, J. M. 1997, ApJS, 108, 155
- Glass, I. S., Moorwood, A. F. M. 1985, MNRAS, 214, 429
- Gregório-Hetem, J., Lépine, J.R.D., Quast, G.R., Torres, C.A.O., de la Reza, R. 1992, AJ, 103, 549
- Hasinger, G. 1998, Astronomische Nachrichten, 319 (astro-ph/9712342)
- Heckman, T. M., 1980, A&A, 87, 152

- Ho, L., Filippenko, A. V., Sargent, W. L. W. 1997, *ApJ*, 487, 568
- Hogg, D. E., Roberts, M. S., Sandage, A. 1993, *AJ*, 106, 907
- Huchra, J. P. 1977, *ApJS*, 35, 171
- Hunt, L. K., Malkan, M. A., Salvati, M., Mandolesi, N., Palazzi, E., Wade, R. 1997, *ApJS*, 108, 229
- Kennicutt, R. C. Jr. 1983, *ApJ*, 272, 54
- Kennicutt, R. C. Jr. 1990, in Paired and interacting galaxies, IAU No. 124, J. W. Sulentic, W. C. Keel, C. M., Telesco, G. C. Marshall, eds., NASA conf. publication, p. 269
- Krügel, E., Tutukov, A. V. 1993, *A&A*, 275, 416
- Larson, R. B. 1990, *PASP*, 102, 709
- Lonsdale, C. J., Helou, G., Good, J. C., Rice, W., 1985, *Cataloged Galaxies and Quasars Observed in the IRAS Survey*, JPL D-1932, Pasadena
- Malkan, M. A., Gorjian, V., Tam, R. 1998, *ApJS*, 117, in press (astro-ph/9803123)
- Maiolino, R., Ruiz, M., Rieke, G. H., Keller, L. D. 1995, *ApJ*, 446, 561
- Meadows, V. S., Allen, D. A., Norris, R. P., Roche, P. F. 1990, *ASA*, 8, 246
- Mirabel, F., & Duc, P. A., 1993, in I. Shlosman (ed.), *Mass-Transfer Induced Activity in Galaxies*, Cambridge University Press, p. 312
- Peña, M., Ruiz, M. T., Maza, J. 1991, *A&A*, 251, 417
- Salzer, J. J., MacAlpine, G. M., Boroson, T. A. 1989, *ApJS*, 70, 447
- Sanders, D. B., Soifer, B. T., Elias, J. H., Madore, B. F., Matthews, K., Neugebauer, G., Scoville, N. Z. 1988, *ApJ*, 325, 74
- Sauvage, M., Thuan, T. X. 1994, *ApJ*, 429, 153
- Searle, L., Sargent, W. L. W. 1972, *ApJ*, 173, 25
- Sekiguchi, K., 1987, *ApJ*, 316, 145
- Stauffer, J. P. 1982, *ApJS*, 50, 517
- Roberts, M. S., Haynes, M. P., 1994, *ArAA*, 32, p. 115
- Taylor, C. L., Brinks, E., Grashuis, R. M., Skillman, E. D. 1996, *ApJS*, 102, 189

- Telles, E., Terlevich, R. J. 1995, MNRAS, 275, 1
- Terlevich, R., Melnick, J., Masegosa, J., Moles, M., Copetti, M. V. F. 1991, A&A, 91, 285
- Torres, C.A.O., Quast, G.R., de la Reza, R., Lépine, J.R.D., Gregório-Hetem, J. 1995. AJ, 109, 2146
- Torres, C.A.O., Quast, G.R., 1995, in Proceedings of the XXIth Annual Meeting of the Sociedade Astronômica Brasileira, F. Jablonski, F. Elizalde, L. Sodré, V. Jatenco-Pereira, eds., p. 139
- van den Bergh, S. V., Abraham, R. G., Ellis, R. S., Tanvir, N. R., Santiago, B. X., Glazebrook, K. 1996, AJ, 112, 359
- Veilleux, S., Osterbrock, D. E. 1987, ApJS, 63, 295
- Veilleux, S., Kim, D. -C., Sanders, D. B., Mazarella, J. M. & Soifer, B. T. 1995, ApJ98, 171
- Véron-Cetty M.-P., Véron P., 1996, A Catalogue of Quasars and Active Galactic Nuclei, 7th ed., ESO Scientific Report 17
- Véron, P., Gonçalves, A. C., Véron-Cetty, M.-P. 1997, A&A, 319, 52
- Voges, W., Aschenbach, B., Boller, Th., Braeuninger, H., Briel, U., Burkert, W., Dennerl, K., Englhauser, J., Gruber, R., Haberl, F., Hartner, G., Hasinger, G., Kuerster M., Pfeffemann, E., Pietsch, W., Predhel, P., Rosso, C., Schmitt, J. H. M. M., Truemper, J., Zimmermann, H. -U. 1996, ROSAT All-Sky Bright Source Catalogue, Max-Planck-Institut fuer extraterrestrische Physik, Garching
- Weedman, D. W., Feldman, F. R., Balzano, V. A., Ramsey, L. W., Sramek, R. A., Chi-Chao Wu 1981, ApJ, 248, 105

Fig. 1.— The FIR vs. B luminosities of a) the PDS starburst candidates, b) the PDS Seyfert galaxies. The diagonal lines correspond to the ratios $L_{\text{IR}}/L_{\text{B}} = 1/3, 1, 3$ and 10. In a), the mean values and dispersions of the luminosities for a sample of normal late-type spirals (sL), early-type spirals (sE) and SBNGs from the literature are indicated. In b), the mean values and dispersions of the luminosities for another sample of normal galaxies (Roberts & Haynes 1994), which is not biased towards emission-line galaxies are also indicated.

Fig. 2.— IRAS color-color diagram for the normal spirals and for different samples of starburst galaxies: the SBNGs, H II galaxies and LIGs. The grid corresponds to a two blackbody model, composed of a cold component at $\sim 27\text{K}$ added to a hot component, associated to a burst of star formation (Sekiguchi 1987). The numbers on the grid indicate the fractional contribution of the hot component to the total FIR luminosity. In a), we call the IRAS Normal galaxies the galaxies with a IPSC color $\alpha(60, 25) < -2.5$ (see section 3.3).

Fig. 3.— The same diagram as in Figure 2 for a) the PDS starbursts, b) the PDS Seyfert galaxies. The locus of a pure power law is also indicated for reference.

Fig. 4.— The color-color diagram $\alpha(60,25)$ vs. $\alpha(25,12)$, showing the distribution of a) the starbursts, b) the AGNs and normal IRAS galaxies. In a), the misidentified AGNs for which we have spectra are identified by crosses. Only 1% of the starbursts have a spectral index $\alpha(60,25) > -1.9$. These galaxies (identified by squares) are at one of the extreme of the sequence traced by the normal and starburst galaxies. In b), most of the Sy1 and X-ray AGNs with a color $\alpha(60,25) > -1.9$ have a color $\alpha(25,12) > -1.5$ as opposed to the Sy2 and X-ray starbursts. Following our definition in section 3.3, the IRAS normal galaxies have a color $\alpha(60,25) < -2.5$.

Fig. 5.— Diagnostic diagram for classifying some of the PDS galaxies. The PDS starbursts with a color $\alpha(60,25) > -1.9$ are identified by a circle with a cross and the capital X represent the X-ray PDS starbursts. 9 of the 12 starbursts with a color $\alpha(60,25) > -1.9$ turn out to be misclassified AGNs (mostly Sy2). The X-ray starbursts, on the other hand, have spectral characteristics suggesting an intermediate nature between one of a LINER and a starburst.

Fig. 6.— Distribution of the morphologies for the PDS starbursts, the Markarian galaxies and the sample of SBNGs from Balzano (1983). The high number of early-type PDS and Markarian galaxies (Sb and earlier) is a trait of SBNGs (Coziol et al. 1997a).

Fig. 7.— FIR luminosities vs. redshifts for the PDS starbursts, as compared to the UV-bright SBNGs

(MBG) and a sample of luminous IRAS starbursts from Allen et al. (1991). The diagonal lines correspond to the flux limits of the different surveys.

Table 1. PDS Starbursts

IRAS	Other names	α (1950)	δ (1950)	z	B	Morph.
00013 + 2028	NGC7817	0 1 24.90	20 28 18.0	0.0083	12.56	SAbc
00022 – 6220	NGC7823	0 2 14.05	-62 20 23.6	0.0148	13.40	SA(s)ab
00073 + 2538	MRK0545, NGC0023	0 7 18.40	25 38 44.0	0.0159	12.85	SB(s)a
00317 – 2142X	MBG00317-2142	0 31 43.70	-21 42 51.0	0.0268	13.66	(R)SB(rl)bc
00344 – 3349	AM0034-344	0 34 25.67	-33 49 49.0	0.0205
00345 – 2945	AM0034-294, NGC174	0 34 30.99	-29 45 10.6	0.0116	13.79	SB(rs)0/a
00386 + 4033	...	0 38 40.39	40 33 40.1	0.0116
00450 – 2533X	NGC0253	0 45 05.75	-25 33 39.8	0.0008	8.04	SAB(s)c
00506 + 7248	MCG+12-02-001	0 50 40.50	72 48 56.0	0.0164
01053 – 1746	MBG01053-1746, IC1623	1 5 18.89	-17 46 22.1	0.0202
01076 – 1707	MCG-03-04-014	1 7 40.84	-17 7 11.5	0.0351	15.00	...
01171 + 0308	ARP227, NGC470	1 17 10.50	3 8 53.0	0.0083	12.53	SA(rs)b
01384 – 7515	AM0138-751, NGC643B	1 38 23.00	-75 15 54.0	0.0127	14.57	SB0
01579 + 5015	UGC01493A	1 57 55.29	50 15 56.0	0.0169	14.40	...
02031 – 8413	AM0203-841	2 3 9.00	-84 13 42.0	0.0108	13.42	SAB(rs)c pec
02070 – 2338	MBG02070-2339, AM0207-233	2 7 0.80	-23 39 3.4	0.0178	13.21	Sbc
02079 + 3725	ARK077, NGC0834	2 8 0.02	37 25 52.0	0.0160	13.84	...
02141 – 1134	MBG02141-1134, NGC873	2 14 6.10	-11 34 48.0	0.0136	13.00	Sc pec
02208 + 4744	UGC1845	2 20 51.23	47 44 36.6	0.0163	14.80	Sab
02315 – 3915	MBG02316-3915, NGC 0986	2 31 34.10	-39 15 49.0	0.0067	11.64	(R)SB(rs)b
02345 + 2053	ARK088, NGC0992, IIZw004	2 34 35.60	20 53 4.0	0.0144	13.65	...
02360 – 0653	NGC1022	2 36 4.30	-6 53 24.0	0.0053	...	(R)SB(s)a
02395 + 3433	KUG0239+345, NGC1050	2 39 32.06	34 33 4.0	0.0137	13.47	(R)SB(s)a
03004 – 2303	MBG03004-2303, NGC1187	3 0 23.80	-23 3 47.0	0.0048	11.34	SB(r)c
03021 + 7956	UGC02519	3 2 10.50	79 56 17.0	0.0086	14.30	Scd
03064 – 0308	MRK0603, NGC1222	3 6 25.70	-3 8 43.0	0.0085	13.10	S0- pec
03266 + 4139	NGC1334	3 26 40.66	41 39 40.0	0.0148	14.10	...

Table 1—Continued

IRAS	Other names	α (1950)	δ (1950)	z	B	Morph.
03324 – 1000	MBG03324-1000, NGC1363	3 32 25.20	-10 0 30.0	0.0321	13.10	...
03344 – 2103	NGC1377	3 34 25.92	-21 3 57.3	0.0060	13.36	S0
03406 + 3908	MRK1405	3 40 38.17	39 8 16.0	0.0165	13.4	S0
03419 + 6756	IC0342	3 41 58.60	67 56 26.0	0.0008	9.10	SAB(rs)cd
03443 – 1642	MCG-03-10-045	3 44 20.77	-16 42 13.6	0.0043	14.00	IB pec
03451 + 6956	UGC02866	3 45 7.10	69 56 37.0	0.0048	15.50	...
03514 + 1546	CGCG 465-012	3 51 26.20	15 46 55.5	0.0227	15.20	Sa
03524 – 2038	NGC1482	3 52 27.11	-20 38 52.4	0.0065	13.10	SA0+ pec
04064 + 0831	NGC1517	4 6 29.00	8 31 1.0	0.0121	14.07	Scd
04296 + 2923	...	4 29 39.91	29 23 39.5	0.0075	12.19	...
04326 + 1904	UGC03094	4 32 38.30	19 4 14.0	0.0253	16.50	...
04389 – 0257	NGC1637	4 38 57.50	-2 57 11.0	0.0027	11.47	SAB(rs)c
04435 + 1822	UGC03157	4 43 35.74	18 22 18.0	0.0159	15.00	...
04519 + 0311	MRK1088, NGC1691	4 52 1.00	3 11 23.0	0.0157	13.01	(R)SB(s)0/a
04569 – 0756	NGC1720	4 56 55.60	-7 55 59.0	0.0144	13.00	SB(s)ab
05053 – 0805	MRK1093, NGC1797	5 5 19.50	-8 4 59.0	0.0151	15.50	(R)SB(rs)a pec
05054 + 1718X	CGCG468-002	5 5 27.39	17 18 13.8	0.0181
05149 – 3709	AM0514-370	5 14 55.00	-37 9 12.0	0.0044	13.04	Sbc
06107 + 7822	NGC2146	6 10 42.16	78 22 27.6	0.0037	11.38	SB(s)ab pec
06141 + 8220	UGC03435	6 14 9.18	82 20 31.9	0.0150	14.72	...
06189 – 2001	UGCA128	6 18 56.00	-20 1 24.0	0.0067
06194 – 5733	AM0619-573, NGC2221	6 19 26.00	-57 33 12.0	0.0081	13.83	SA pec
06210 + 4932	CGCG233-017	6 21 3.58	49 32 13.0	0.0202	14.90	...
06259 – 4708	AM0626-470	6 26 0.00	-47 8 36.0	0.0392	19.26	...
06399 – 5828	AM0639-582	6 39 57.00	-58 28 36.0	0.0086	13.10	(R)SAB(s)bc
07007 + 8427	NGC2268	7 0 52.70	84 27 45.0	0.0081	12.24	SAB(r)bc
07027 – 6011	AM0702-601	7 2 44.50	-60 11 6.0	0.0309

Table 1—Continued

IRAS	Other names	α (1950)	δ (1950)	z	B	Morph.
07107 + 3521	UGC03752	7 10 45.14	35 21 55.0	0.0163	14.80	...
07176 – 3533	ESO367-G017	7 17 38.00	-35 33 48.0	0.0092	13.85	(R)SB(rl)a
07203 + 5803	UGC03828	7 20 21.50	58 4 1.0	0.0124	12.90	SAB(rs)b
07204 + 3332	MRK1199, UGC03829	7 20 28.30	33 32 20.7	0.0143	13.70	Sc
07256 + 3355	GC2388	7 25 38.17	33 55 17.4	0.0144	14.67	...
07278 – 6728	AM0727-672, IC2202	7 27 50.00	-67 28 12.0	0.0116	13.61	SAB(s)bc
07369 – 5504	AM0737-550	7 36 59.00	-55 4 30.0	0.0091	11.85	SB(s)b
07568 + 1531	UGC04145	7 56 50.30	15 31 30.0	0.0159	14.06	Sa
08007 – 6600	...	8 0 43.59	-66 0 51.9	0.0407	16.18	pec
08311 – 2248	AM0831-224, NGC2613	8 31 11.10	-22 48 1.0	0.0057	11.16	SA(s)b
08339 + 6517X	...	8 33 57.30	65 17 45.0	0.0191	14.16	...
08406 – 1952	ESO563-G014	8 40 41.70	-19 52 19.0	0.0058	14.00	SBd
08425 + 7416	ARP080, NGC2633	8 42 33.80	74 16 54.0	0.0079	12.90	SB(s)b
08437 – 1907	NGC2665	8 43 45.00	-19 7 12.0	0.0058	13.50	(R)SB(r)a
09004 – 2031	ESO564-G011	9 0 30.00	-20 31 36.0	0.0088	14.50	Sa
09120 + 4107	NGC2785	9 12 3.07	41 7 32.6	0.0098	14.73	Im
09141 + 4212	ARP283, NGC2798	9 14 9.41	42 12 34.0	0.0064	13.04	SB(s)a pec
09395 + 0454	MRK0708, NGC2966	9 39 34.54	4 54 6.5	0.0072	13.56	...
09399 + 3204	MRK0404, NGC2964	9 39 56.90	32 4 34.0	0.0048	12.00	SAB(r)bc
09434 – 1408	ARP245, NGC2993	9 43 24.01	-14 08 12.6	0.0081	13.11	Sa pec
09479 + 3347	KUG0947+337, NGC3021	9 47 59.60	33 47 18.0	0.0058	12.91	SA(rs)bc
09510 + 0149	NGC3044	9 51 6.00	1 48 57.0	0.0047	12.46	SB(s)c
09511 – 1214	NGC3058	9 51 10.43	-12 14 45.1	0.0250
09517 + 6955X	M082	9 51 43.48	69 55 00.8	0.0007	9.3	I0
09578 + 0336	UGC05376	9 57 51.10	3 36 56.0	0.0072	14.02	Sdm
09593 + 6858	NGC3077	9 59 19.95	68 58 29.9	0.0007	10.61	I0 pec
10102 + 1716	NGC3154	10 10 18.00	17 16 58.0	0.0225

Table 1—Continued

IRAS	Other names	α (1950)	δ (1950)	z	B	Morph.
10138 + 2122	NGC3177	10 13 49.20	21 22 28.0	0.0049	13.04	SA(rs)b
10153 + 2205	ARP316, NGC3189	10 15 20.64	22 4 54.9	0.0049	12.12	SA(s)a pec
10257 – 4338X	AM1025-433, NGC3256	10 25 43.40	-43 38 48.0	0.0091	12.15	...
10270 – 4351	AM1027-435, NGC3263	10 27 4.50	-43 51 59.0	0.0093	12.50	SB(rs)cd
10292 – 4148	ESO317-G041	10 29 12.00	-41 48 12.0	0.0191	14.38	SB(r)bc pec
10356 + 5345X	ARP217, NGC3310	10 35 40.10	53 45 49.0	0.0033	11.15	SAB(r)bc pec
10409 – 4556	ESO264-G036	10 40 57.00	-45 56 54.0	0.0231	14.30	SB(s)b
10484 – 0152	ARK258, IC0651	10 48 25.30	-1 53 4.0	0.0152	13.60	SB(s)m pec
10560 + 6147	MRK0158, NGC3471	10 56 2.20	61 47 56.0	0.0078	13.23	Sa
10567 – 4310	AM1056-430	10 56 44.00	-43 10 24.0	0.0170	14.97	SA(rs)bc
11004 + 2814	KUG1100+282, NGC3504	11 0 28.50	28 14 31.0	0.0057	11.67	(R)SAB(s)ab
11005 – 1601	NGC3508	11 0 30.80	-16 1 9.0	0.0131	13.20	SA(r)b pec
11082 – 4849	ESO215-G031	11 8 18.00	-48 49 54.0	0.0088	13.64	(R)SB(r)b
11122 – 2327	AM1112-232, NGC3597	11 12 14.20	-23 27 20.0	0.0117	13.60	S0+ pec
11149 + 0449	NGC3611	11 14 54.70	4 49 41.0	0.0057	12.77	SA(s)a pec
11186 – 0242	CGCG011-076	11 18 39.08	-2 42 36.5	0.0252	14.78	SAB(s)b
11257 + 5850X	MRK0171, NGC3690	11 25 41.40	58 50 15.4	0.0104	11.8	SBm pec
11330 + 7048	NGC3735	11 33 4.80	70 48 42.0	0.0097	12.50	SAc
11442 – 2738	AM1144-273, NGC3885	11 44 15.00	-27 38 42.0	0.0060	11.89	SAB(r)0/a
12015 + 3210	KUG1201+321, NGC4062	12 1 30.50	32 10 26.0	0.0032	11.90	SA(s)c
12038 + 5259	NGC4102	12 3 51.66	52 59 23.7	0.0035	11.99	SAB(s)b
12063 + 7511	NGC4133	12 6 24.80	75 10 52.0	0.0052	13.11	SABb
12080 + 1618	MRK0759, NGC4152	12 8 4.44	16 18 40.8	0.0077	12.66	SAB(rs)c
12115 – 4656	AM1211-465	12 11 34.80	-46 57 2.0	0.0182	14.17	SA(rs)ab
12116 + 5448X	MRK0201, NGC4194, IZw033	12 11 41.20	54 48 15.0	0.0090	13.01	IBm pec
12121 – 3513	AM1212-351	12 12 8.00	-35 13 54.0	0.0089	12.96	SB(rs)b
12142 – 4841	...	12 14 12.79	-48 41 39.2	0.0177	16.20	E

Table 1—Continued

IRAS	Other names	α (1950)	δ (1950)	z	B	Morph.
12173 + 0537	NGC4273	12 17 22.74	5 37 13.0	0.0083	12.39	SB(s)c
12190 + 1452	NGC4298	12 19 0.55	14 53 1.1	0.0043	12.04	SA(rs)c
12193 – 4303	AM1219-430	12 19 18.00	-43 3 24.0	0.0234
12204 + 6607	NGC4332	12 20 27.60	66 7 15.0	0.0102	13.12	SB(s)a
12221 + 3939	MRK0439, NGC4369	12 22 8.03	39 39 35.0	0.0041	12.33	(R)SA(rs)a
12290 + 5814	MRK0213, NGC4500	12 29 2.60	58 14 26.0	0.0112	13.10	SB(s)a
12319 + 0227	NGC4536	12 31 53.81	2 27 50.5	0.0064	11.16	SAB(rs)bc
12351 – 4015	NGC4575	12 35 9.00	-40 15 42.0	0.0098	13.12	SAB(rs)bc
12398 – 0641	MRK1333, NGC4628	12 39 50.14	-6 41 50.4	0.0097	14.50	SA(s)b
12456 – 0303	NGC4691	12 45 39.02	-3 3 36.9	0.0040	11.66	(R)SB(s)0/a pec
12498 – 3845	MCG-06-28-02	12 49 53.00	-38 45 24.0	0.0141	13.29	(R)SA(rs)b
12542 – 0815	NGC4818	12 54 12.70	-8 15 13.0	0.0041	12.00	SAB(rs)ab pec
12596 – 1529	MCG-02-33-098	12 59 40.80	-15 29 58.0	0.0160	14.50	Sc pec
13063 – 1515	NGC4984	13 6 18.20	-15 15 1.0	0.0042	12.25	(R)SAB(rs)0+
13078 – 4117	ESO323-G090	13 7 47.00	-41 17 36.0	0.0102	13.92	SB(rs)0+
13109 – 4912	ESO219-G041	13 11 0.00	-49 12 54.0	0.0115	12.90	(R)SB(s)ab
13136 + 6223	ARP238	13 13 42.14	62 23 16.2	0.0317	15.00	Sc
13166 – 1434	NGC5073	13 16 41.20	-14 34 50.0	0.0093	13.00	SB(s)c
13286 – 3432	AM1328-343, NGC5188	13 28 37.00	-34 32 18.0	0.0077	12.96	(R)SAB(rs)b
13301 – 2356	AM1330-235, IC4280	13 30 7.90	-23 57 1.0	0.0165	13.46	...
13304 + 6301	ARP104, NGC5218	13 30 27.80	63 1 27.0	0.0102	13.10	SB(s)b pec
13341 – 2936X	M083	13 34 11.55	-29 36 42.2	0.0017	8.20	SAB(s)c
13370 – 3123	AM1337-312, NGC5253	13 37 5.12	-31 23 13.2	0.0013	10.87	Im pec
13373 + 0105	ARP240, NGC5258	13 37 24.60	1 5 6.0	0.0228	12.93	SA(s)b pec
13478 – 4848	ESO221-IG010	13 47 48.00	-48 48 30.0	0.0101
13549 + 4205	MRK0281, NGC5383	13 54 59.99	42 5 22.3	0.0081	12.05	(R)SB(rs)b pec
13591 + 5934	MRK0799, NGC5430	13 59 8.50	59 34 16.0	0.0108	12.72	SB(s)b

Table 1—Continued

IRAS	Other names	α (1950)	δ (1950)	z	B	Morph.
14179 – 4604	IC4402	14 18 0.00	-46 4 12.0	0.0053	12.00	Sb
14187 + 7149	MRK0286, NGC5607, VIIZw547	14 18 49.60	71 49 3.0	0.0260	13.90	Pec
14280 + 3126	NGC5653	14 28 1.00	31 26 10.0	0.0125	12.86	(R)SA(rs)b
14299 + 0818	ARP049, NGC5665	14 29 57.70	8 17 58.0	0.0078	12.66	SAB(rs)c pec
14376 – 0004	NGC5713	14 37 37.56	-0 04 29.0	0.0063	11.84	SAB(rs)bc pec
14430 – 3728	ESO386-G019	14 43 2.80	-37 28 32.0	0.0148	13.65	SA(r)0/a
14454 – 4343	ESO273-IG004	14 45 26.00	-43 43 24.0	0.0386
14483 + 0519	NGC5765	14 48 20.76	5 19 17.7	0.0015
14544 – 4255	AM1454-425, IC4518A	14 54 26.00	-42 55 48.0	0.0160	15.00	Sc pec
14545 – 1900	IC1077	14 54 32.00	-19 0 54.0	0.0116	13.44	SA(s)bc
14556 – 4148	NGC5786	14 55 41.00	-41 48 48.0	0.0098	12.00	(R)SAB(s)bc
15005 + 8343	MRK0839	15 0 32.68	83 43 16.2	0.0136	13.82	...
15042 – 3608	NGC5843	15 4 19.00	-36 8 12.0	0.0139	13.11	SB(s)b
15153 + 5535	NGC5908	15 15 23.00	55 35 37.0	0.0117	12.79	SA(s)b
15188 – 1254	NGC5915	15 18 47.50	-12 54 47.0	0.0077	12.75	SB(s)ab pec
15243 + 4150	IZw112, ARP090, NGC5930	15 24 20.73	41 51 0.1	0.0095	13.60	SAB(rs)b pec
15268 – 7757	ESO022-G010	15 26 52.00	-77 57 18.0	0.0084	13.72	S0
15276 + 1309	NGC5936	15 27 39.70	13 9 40.0	0.0138	13.11	SB(rs)b
15281 – 0239	NGC5937	15 28 9.90	-2 39 33.0	0.0095	13.17	(R)SAB(rs)b pec
15347 + 4341	IC4564	15 34 44.60	43 40 57.0	0.0195	14.42	...
15420 – 7531	AM1542-753, NGC5967	15 42 6.00	-75 31 6.0	0.0092	12.70	SAB(rs)c
15437 + 0234	NGC5990	15 43 44.80	2 34 11.0	0.0131	13.30	(R)Sa pec
15467 – 2914X	NGC6000	15 46 44.30	-29 14 06.0	0.0070	13.01	SB(s)bc
15496 + 4724	UGC10070	15 49 40.32	47 24 14.0	0.0205	13.98	...
16030 + 2040	MRK0297, NGC6052	16 3 1.40	20 40 37.0	0.0162
16037 + 2137	NGC6060	16 3 41.60	21 37 8.0	0.0153	13.80	SAB(rs)c
16104 + 5235	MRK0496, NGC6090, IZw135	16 10 24.02	52 35 4.1	0.0300

Table 1—Continued

IRAS	Other names	α (1950)	δ (1950)	z	B	Morph.
16180 + 3753	IZw141, NGC6120	16 18 1.19	37 53 36.0	0.0312	14.60	Pec
16284 + 0411	CGCG052-037	16 28 27.00	4 11 24.0	0.0248	15.04	...
16301 + 1955	NGC6181	16 30 9.40	19 55 48.0	0.0084	12.49	SAB(rs)c
16516 – 0948	...	16 51 39.65	-9 48 31.3	0.0227	16.55	Sc
17091 + 0803	UGC10743	17 9 6.20	8 3 16.0	0.0089	14.74	Sa
17138 – 1017	...	17 13 50.10	-10 17 25.0	0.0177	16.57	...
17222 – 5953	AM1722-595	17 22 16.00	-59 53 24.0	0.0203	13.74	Sbc
17363 + 8646	MRK1116, VIIZw729	17 36 22.70	86 46 38.8	0.0264	14.30	...
17442 – 6314	IC4664	17 44 13.00	-63 14 18.0	0.0163	13.64	(R)SAB(r)b
17467 + 0807	CGCG 055-018	17 46 42.66	8 7 1.8	0.0211	15.5	...
17530 + 3447	ARK534	17 53 4.42	34 47 0.8	0.0167	14.10	Sab
18093 – 5744	AM1809-574, IC4687	18 9 20.10	-57 44 20.0	0.0170	14.31	Sb pec
18095 + 1458	NGC6574	18 9 34.70	14 58 3.0	0.0080	12.83	SAB(rs)bc
18097 – 6006	AM1809-600	18 9 47.00	-60 6 24.0	0.0102	13.55	(R)SAB(rs)a
18131 + 6820	VIIZw778, ARP081, NGC6621	18 13 9.01	68 20 52.5	0.0213	14.00	Sb pec
18262 + 2242	UGC11246	18 26 16.88	22 42 9.2	0.0143	14.90	Sab
18293 – 3413	...	18 29 21.38	-34 13 41.5	0.0180
18329 + 5950	VIIZw812, NGC6670A	18 32 57.44	59 50 57.1	0.0296	15.70	...
18375 – 4150	ESO336-G009	18 37 35.00	-41 50 30.0	0.0192	14.00	SB(s)b
18425 + 6036	NGC6701	18 42 35.12	60 36 4.0	0.0139	13.01	(R)SB(s)a
19070 + 5051	NGC6764	19 7 1.22	50 51 8.1	0.0087	12.56	SB(s)bc
19265 – 4338	...	19 26 34.51	-43 38 56.8	0.0595	15.80	...
19384 – 7045	NGC6808	19 38 28.00	-70 45 6.0	0.0111	12.46	SA(r)ab pec
19517 – 1241	NGC6835	19 51 46.10	-12 42 4.0	0.0055	13.41	SB(s)a
19582 – 3833	AM1958-383	19 58 14.50	-38 33 9.0	0.0166	13.54	SA(rs)ab
20192 + 6634	NGC6911	20 19 12.15	66 34 6.6	0.0090	15.10	SBb
20243 – 0226	IIZw083	20 24 20.10	-2 26 34.6	0.0294	15.20	...

Table 1—Continued

IRAS	Other names	α (1950)	δ (1950)	z	B	Morph.
20272 – 4738	NGC6918	20 27 15.00	-47 38 24.0	0.0057	14.42	(R)SAB(rs)a
20338 + 5958X	ARP029, NGC6946	20 33 49.24	59 58 49.2	0.0002	9.61	SAB(rs)cd
20550 + 1655	IIZw096	20 55 5.30	16 56 3.0	0.0363
20551 – 4250	AM2055-425	20 55 8.82	-42 50 45.1	0.0426	14.74	Merger
21008 – 4347	ESO286-G035	21 0 52.83	-43 47 31.1	0.0171	15.00	...
21087 + 6557	UGC11689	21 8 45.11	65 57 50.9	0.0103	14.40	SB(r)b
21171 – 0859	NGC7051	21 17 10.55	-8 59 41.4	0.0086	14.00	SB(r)a pec
21330 – 3846	AM2133-384	21 33 5.65	-38 46 0.5	0.0192	15.07	pec
21457 – 8145	AM2145-814	21 45 48.00	-81 45 54.0	0.0080	12.23	SB(s)c
23179 + 1657	IIIZw102, NGC7625	23 17 59.90	16 57 6.0	0.0058	12.83	SA(rs)a pec
23192 – 4245	AM2319-424, NGC7632	23 19 16.55	-42 45 14.9	0.0048	12.95	(RL)SB(1)0+
23256 + 2315	MRK0326, NGC7677	23 25 36.50	23 15 22.0	0.0123	13.93	SAB(r)bc
23336 + 0152X	MRK0538, NGC7714	23 33 40.58	1 52 42.3	0.0093	13.00	SB(s)b pec
23568 + 2028	MRK0332, NGC7798	23 56 52.00	20 28 17.0	0.0084	12.97	...

Table 2. PDS starbursts Optical–FIR characteristics

IRAS	M_B	$\text{Log}(L_B/L_\odot)$	$\text{Log}(L_{IR}/L_\odot)$	$\alpha(25,12)$	$\alpha(60,25)$	$\alpha(100,60)$	quality
00013 + 2028	-20.18	9.96	10.10	-0.15	-2.44	-2.10	3332
00022 – 6220	-20.46	10.07	10.37	-0.81	-2.46	-1.32	3332
00073 + 2538	-21.30	10.41	10.80	-0.99	-2.45	-1.00	3232
00317 – 2142	-21.56	10.51	10.95	-1.27	-2.21	-1.53	3332
00344 – 3349	10.78	-2.44	-1.09	0.50	3332
00345 – 2945	-21.14	10.35	10.61	-1.58	-2.49	-0.99	3332
00386 + 4033	0.09	-2.31	-2.68	2322
00450 – 2533	-19.83	9.82	10.20	-2.19	-2.15	-0.46	3332
00506 + 7248	11.17	-2.15	-2.05	-0.34	3222
01053 – 1746	11.38	-2.26	-2.11	-0.58	3332
01076 – 1707	-20.79	10.20	11.35	-1.41	-2.33	-0.93	3332
01171 + 0308	-20.15	9.95	10.11	-1.18	-2.09	-1.31	3232
01384 – 7515	-19.13	9.54	10.53	-1.21	-2.51	-1.25	3332
01579 + 5015	-20.96	10.27	10.53	-1.24	-2.10	-0.75	3322
02031 – 8413	-20.20	9.97	10.15	-0.71	-2.47	-1.89	3332
02070 – 2338	-21.06	10.31	10.58	-0.22	-2.42	-1.85	3332
02079 + 3725	-20.34	10.02	10.68	-0.96	-2.46	-1.30	3332
02141 – 1134	-20.70	10.17	10.51	-0.73	-2.37	-1.33	2232
02208 + 4744	-20.57	10.12	10.83	-1.37	-2.64	-0.60	3322
02315 – 3915	-22.07	10.71	10.46	-1.77	-2.28	-1.36	3332
02345 + 2053	-20.56	10.11	10.76	-1.06	-2.42	-0.89	3332
02360 – 0653	10.16	-2.07	-2.09	-0.57	3332
02395 + 3433	-20.42	10.06	10.45	-2.08	-1.71	-0.71	3332
03004 – 2303	-20.10	9.93	9.85	-1.37	-2.28	-1.48	3332
03021 + 7956	-19.29	9.61	9.84	-0.58	-2.46	-1.89	3322
03064 – 0308	-19.68	9.76	10.35	-2.03	-2.04	-0.28	3332
03266 + 4139	-20.86	10.23	10.48	-0.55	-2.48	-1.47	3322
03324 – 1000	-22.51	10.89	11.08	-0.62	-2.39	-1.48	3332

Table 2—Continued

IRAS	M_B	$\text{Log}(L_B/L_\odot)$	$\text{Log}(L_{IR}/L_\odot)$	$\alpha(25,12)$	$\alpha(60,25)$	$\alpha(100,60)$	quality
03344 – 2103	-18.61	9.33	9.76	-1.92	-1.58	0.46	3332
03406 + 3908	-21.83	10.62	10.60	-0.53	-2.54	-1.44	3322
03419 + 6756	-21.87	10.64	9.18	-2.26	-1.69	-0.89	3322
03443 – 1642	-17.31	8.81	9.37	-1.60	-2.34	-0.98	3332
03451 + 6956	-17.63	8.94	10.33	-1.84	-2.06	-0.46	3322
03514 + 1546	-20.65	10.15	10.89	-1.21	-2.32	-0.79	3332
03524 – 2038	-19.05	9.51	10.54	-1.47	-2.23	-0.68	3332
04064 + 0831	-19.87	9.84	10.16	-0.60	-2.53	-1.49	3322
04296 + 2923	-21.61	10.53	10.71	-2.17	-2.12	-0.32	3322
04326 + 1904	-19.99	9.88	11.08	-1.01	-2.36	-1.34	3322
04389 – 0257	-18.85	9.43	9.14	-1.29	-1.94	-1.84	3332
04435 + 1822	-20.37	10.04	10.49	-1.19	-1.88	-1.94	3322
04519 + 0311	-21.19	10.36	10.65	-1.56	-2.36	-0.96	3332
04569 – 0756	-21.00	10.29	10.62	-1.22	-2.58	-1.36	3322
05053 – 0805	-18.61	9.33	10.71	-1.89	-2.09	-0.93	3322
05054 + 1718	10.94	-2.19	-2.55	-0.35	3322
05149 – 3709	-18.29	9.20	9.30	-0.18	-2.65	-2.06	3332
06107 + 7822	-19.76	9.79	10.65	-1.41	-2.29	-0.67	3332
06141 + 8220	-19.42	9.65	10.42	-1.10	-2.27	-1.02	3332
06189 – 2001	9.85	-0.81	-2.33	-1.68	3322
06194 – 5733	-18.89	9.44	9.98	-1.22	-2.46	-1.59	3332
06210 + 4932	-20.25	9.99	10.65	-0.56	-2.49	-1.52	3322
06259 – 4708	-16.85	8.63	11.55	-2.05	-2.06	-0.67	3332
06399 – 5828	-19.93	9.86	10.01	-0.49	-2.48	-1.85	3332
07007 + 8427	-20.51	10.09	10.05	-0.39	-2.47	-2.02	3332
07027 – 6011	11.16	-1.70	-2.13	-0.80	3332
07107 + 3521	-19.52	9.69	10.15	-1.20	-1.32	-0.64	3322
07176 – 3533	-20.14	9.95	9.93	-1.11	-2.36	-1.20	3322

Table 2—Continued

IRAS	M_B	$\text{Log}(L_B/L_\odot)$	$\text{Log}(L_{IR}/L_\odot)$	$\alpha(25,12)$	$\alpha(60,25)$	$\alpha(100,60)$	quality
07203 + 5803	-20.74	10.18	10.25	-0.88	-2.22	-1.91	3332
07204 + 3332	-20.27	10.00	10.55	-2.06	-1.96	-0.29	3332
07256 + 3355	-19.36	9.63	10.94	-2.08	-2.33	-0.77	3332
07278 – 6728	-20.38	10.04	9.81	-0.68	-1.73	-2.38	3332
07369 – 5504	-21.43	10.46	10.15	-0.70	-2.52	-1.95	3322
07568 + 1531	-20.05	9.91	10.39	-1.35	-1.72	-0.98	3332
08007 – 6600	-20.53	10.10	11.16	-1.76	-1.38	0.34	3322
08311 – 2248	-20.96	10.27	9.93	-0.18	-2.30	-2.73	3322
08339 + 6517	-20.47	10.08	10.75	-1.91	-1.92	-0.19	3332
08406 – 1952	-18.25	9.19	9.50	0.01	-2.72	-2.39	3322
08425 + 7416	-19.65	9.75	10.43	-1.68	-2.21	-0.98	3332
08437 – 1907	-18.70	9.37	9.74	-1.70	-2.03	-0.86	3322
09004 – 2031	-18.90	9.45	10.23	-2.05	-2.24	-0.42	3322
09120 + 4107	-18.23	9.18	10.37	-1.00	-2.45	-1.20	3332
09141 + 4212	-19.02	9.50	10.31	-1.86	-2.08	-0.85	3332
09395 + 0454	-18.83	9.42	9.85	-1.51	-2.24	-0.64	3332
09399 + 3204	-19.45	9.67	9.91	-0.97	-2.49	-1.35	3332
09434 – 1408	-19.73	9.78	10.31	-1.78	-2.19	-0.90	3332
09479 + 3347	-18.90	9.45	9.63	-0.21	-2.71	-1.79	3332
09510 + 0149	-18.95	9.47	9.78	-0.91	-2.54	-1.33	3332
09511 – 1214	10.88	-1.10	-2.39	-1.66	3332
09517 + 6955	-19.52	9.70	10.67	-2.10	-1.60	-0.11	3332
09578 + 0336	-18.29	9.20	9.88	-0.95	-2.41	-1.53	3332
09593 + 6858	-16.98	8.68	8.33	-1.69	-2.24	-1.30	3332
10102 + 1716	10.85	-0.30	-2.53	-1.18	3332
10138 + 2122	-18.48	9.28	9.78	-0.87	-2.44	-1.18	3332
10153 + 2205	-19.41	9.65	9.44	-0.15	-2.52	-2.26	3232
10257 – 4338	-21.17	10.35	11.24	-2.18	-1.95	-0.52	3322

Table 2—Continued

IRAS	M_B	$\text{Log}(L_B/L_\odot)$	$\text{Log}(L_{IR}/L_\odot)$	$\alpha(25,12)$	$\alpha(60,25)$	$\alpha(100,60)$	quality
10270 – 4351	-20.90	10.25	10.30	-0.81	-2.33	-1.91	3322
10292 – 4148	-20.56	10.11	10.61	-1.08	-2.16	-1.44	3322
10356 + 5345	-19.85	9.83	10.07	-1.90	-2.17	-0.49	3332
10409 – 4556	-21.38	10.44	10.96	-0.76	-2.41	-1.70	3322
10484 – 0152	-20.39	10.04	10.51	-0.90	-2.42	-1.53	3332
10560 + 6147	-19.24	9.58	10.10	-1.82	-2.15	-0.96	3332
10567 – 4310	-19.96	9.87	10.68	-1.14	-2.25	-1.16	3322
11004 + 2814	-20.15	9.95	10.26	-1.71	-1.98	-0.85	3332
11005 – 1601	-20.53	10.10	10.54	-1.06	-2.31	-1.43	3232
11082 – 4849	-19.86	9.83	10.07	-1.00	-2.39	-1.09	3322
11122 – 2327	-19.96	9.87	10.64	-1.52	-2.12	-0.72	3332
11149 + 0449	-19.14	9.54	9.61	-1.05	-2.22	-0.97	3232
11186 – 0242	-20.36	10.03	10.99	-1.09	-2.24	-1.20	3322
11257 + 5850	-21.44	10.47	11.48	-2.46	-1.71	-0.07	3332
11330 + 7048	-20.45	10.07	10.33	-0.62	-2.14	-1.98	3332
11442 – 2738	-20.36	10.03	10.02	-1.32	-2.63	-0.47	3232
12015 + 3210	-18.62	9.34	9.02	-0.12	-2.28	-2.81	3332
12038 + 5259	-18.74	9.38	10.16	-2.04	-2.21	-0.78	3332
12063 + 7511	-18.61	9.33	9.57	-1.32	-2.36	-1.43	3332
12080 + 1618	-19.83	9.82	9.86	-0.80	-2.33	-1.47	3232
12115 – 4656	-20.60	10.13	10.69	-0.98	-2.36	-1.06	3322
12116 + 5448	-19.78	9.80	10.63	-2.24	-1.83	-0.37	3332
12121 – 3513	-20.09	9.92	10.39	-2.12	-2.20	-0.70	3332
12142 – 4841	-18.61	9.33	10.49	-0.43	-2.47	-1.55	3322
12173 + 0537	-20.22	9.98	10.30	-0.83	-2.31	-1.62	2232
12190 + 1452	-19.18	9.56	9.60	-0.30	-2.67	-2.80	3332
12193 – 4303	10.87	-0.81	-2.51	-1.13	3222
12204 + 6607	-19.93	9.86	10.31	-1.61	-2.31	-1.30	3332

Table 2—Continued

IRAS	M_B	$\text{Log}(L_B/L_\odot)$	$\text{Log}(L_{IR}/L_\odot)$	$\alpha(25,12)$	$\alpha(60,25)$	$\alpha(100,60)$	quality
12221 + 3939	-18.76	9.39	9.46	-1.15	-2.44	-1.22	3332
12290 + 5814	-20.15	9.95	10.11	-1.07	-2.13	-0.83	3332
12319 + 0227	-20.87	10.23	10.49	-1.28	-2.44	-0.68	3332
12351 - 4015	-20.31	10.01	10.32	-0.84	-2.44	-1.59	3332
12398 - 0641	-18.49	9.28	9.92	-1.15	-1.75	-1.17	3232
12456 - 0303	-19.37	9.64	9.77	-1.66	-2.06	-0.66	3332
12498 - 3845	-20.66	10.15	10.27	-0.15	-2.49	-1.93	3332
12542 - 0815	-19.14	9.54	9.91	-2.08	-1.88	-0.45	3332
12596 - 1529	-19.57	9.71	10.67	-1.89	-1.93	-0.41	2332
13063 - 1515	-18.92	9.45	9.67	-1.17	-2.13	-0.53	3332
13078 - 4117	-19.49	9.68	10.15	-1.04	-2.53	-0.74	3332
13109 - 4912	-21.32	10.41	10.03	-0.43	-2.13	-2.33	3322
13136 + 6223	-20.55	10.11	11.42	-2.36	-1.94	-0.19	3332
13166 - 1434	-19.96	9.87	10.33	-1.84	-2.42	-0.73	3232
13286 - 3432	-19.63	9.74	10.53	-1.64	-2.37	-0.90	3332
13301 - 2356	-20.92	10.26	10.67	-0.65	-2.59	-1.23	3332
13304 + 6301	-19.99	9.88	10.33	-1.72	-2.31	-1.40	3332
13341 - 2936	-21.08	10.32	9.97	-1.91	-1.97	-1.49	3332
13370 - 3123	-17.88	9.04	9.05	-2.08	-1.07	0.07	3332
13373 + 0105	-21.88	10.64	11.17	-1.06	-2.31	-1.46	3332
13478 - 4848	10.54	-1.26	-2.32	-0.84	3322
13549 + 4205	-20.51	10.09	10.05	-0.91	-2.25	-2.03	3232
13591 + 5934	-20.46	10.07	10.54	-1.45	-2.12	-1.23	3332
14179 - 4604	-20.06	9.91	9.81	-1.22	-2.24	-1.31	3322
14187 + 7149	-21.23	10.38	10.91	-1.61	-2.08	-0.89	3332
14280 + 3126	-20.63	10.14	10.69	-0.82	-2.44	-1.26	3332
14299 + 0818	-19.86	9.83	10.05	-1.09	-2.42	-1.31	3332
14376 - 0004	-20.37	10.04	10.38	-1.17	-2.33	-1.18	3332

Table 2—Continued

IRAS	M_B	$\text{Log}(L_B/L_\odot)$	$\text{Log}(L_{IR}/L_\odot)$	$\alpha(25,12)$	$\alpha(60,25)$	$\alpha(100,60)$	quality
14430 – 3728	-20.51	10.09	10.52	-1.05	-2.42	-0.73	3322
14454 – 4343	11.23	-1.88	-1.16	-0.06	3322
14483 + 0519	8.32	-1.29	-1.71	-1.07	3332
14544 – 4255	-19.54	9.70	10.73	-1.82	-2.01	-1.02	3322
14545 – 1900	-20.22	9.98	10.24	-0.84	-2.40	-1.33	3332
14556 – 4148	-21.31	10.41	10.22	-0.73	-2.40	-1.75	3322
15005 + 8343	-20.05	9.91	10.40	-1.53	-1.99	-0.83	3332
15042 – 3608	-20.92	10.26	10.30	-0.60	-2.53	-1.88	3322
15153 + 5535	-20.57	10.12	10.36	-0.47	-2.46	-2.68	3332
15188 – 1254	-20.25	9.99	10.20	-1.54	-2.29	-0.77	3332
15243 + 4150	-19.37	9.64	10.32	-1.97	-2.01	-0.67	3332
15268 – 7757	-19.28	9.60	9.86	-1.54	-2.08	-0.79	3322
15276 + 1309	-20.69	10.16	10.67	-1.31	-2.19	-1.25	3332
15281 – 0239	-20.11	9.93	10.42	-0.78	-2.45	-1.44	3332
15347 + 4341	-20.13	9.94	10.28	-0.48	-2.43	-1.96	3332
15420 – 7531	-20.42	10.06	9.92	-0.68	-2.31	-2.11	3322
15437 + 0234	-20.59	10.12	10.64	-1.27	-2.03	-1.01	3332
15467 – 2914	-19.89	9.84	10.65	-1.91	-2.23	-0.77	3322
15496 + 4724	-20.64	10.14	10.73	-0.22	-2.50	-2.02	3332
16030 + 2040	10.65	-1.51	-2.29	-0.99	3332
16037 + 2137	-20.32	10.02	10.13	-0.07	-2.08	-2.30	3332
16104 + 5235	11.19	-1.97	-2.05	-0.58	3332
16180 + 3753	-20.88	10.24	11.07	-0.98	-2.38	-1.37	3332
16284 + 0411	-20.20	9.97	11.09	-1.33	-2.51	-1.09	3332
16301 + 1955	-20.37	10.04	10.29	-0.90	-2.45	-1.59	3332
16516 – 0948	-19.24	9.58	10.95	-0.88	-2.78	-1.76	3322
17091 + 0803	-18.31	9.21	9.76	-1.12	-2.31	-0.65	3332
17138 – 1017	-19.17	9.56	11.07	-1.65	-2.28	-0.44	3322

Table 2—Continued

IRAS	M_B	$\text{Log}(L_B/L_\odot)$	$\text{Log}(L_{IR}/L_\odot)$	$\alpha(25,12)$	$\alpha(60,25)$	$\alpha(100,60)$	quality
17222 – 5953	-21.15	10.35	11.00	-1.78	-2.30	-0.32	3322
17363 + 8646	-21.03	10.30	11.00	-0.62	-2.59	-1.42	3332
17442 – 6314	-20.76	10.19	10.31	-0.23	-2.23	-2.11	3322
17467 + 0807	-19.79	9.80	10.49	-1.40	-1.23	0.05	3322
17530 + 3447	-20.19	9.96	10.70	-0.70	-2.47	-1.51	3332
18093 – 5744	-20.20	9.97	11.08	-1.78	-2.12	-0.98	3322
18095 + 1458	-20.53	10.10	10.41	-0.94	-2.40	-1.47	3322
18097 – 6006	-19.89	9.84	10.21	-1.42	-1.96	-0.98	3322
18131 + 6820	-20.87	10.24	10.93	-1.68	-2.21	-1.16	3322
18262 + 2242	-19.56	9.71	10.40	-1.10	-2.39	-1.36	3322
18293 – 3413	11.47	-1.65	-2.52	-0.73	2322
18329 + 5950	-19.86	9.83	11.33	-1.45	-2.38	-1.20	3332
18375 – 4150	-20.76	10.19	10.50	-0.31	-2.20	-1.43	3322
18425 + 6036	-20.95	10.27	10.77	-1.34	-2.44	-1.40	3332
19070 + 5051	-20.39	10.04	10.13	-1.74	-1.82	-1.19	3322
19265 – 4338	-21.42	10.46	10.83	-0.74	-0.57	-0.68	3332
19384 – 7045	-21.07	10.32	10.46	-0.59	-2.37	-1.97	3332
19517 – 1241	-18.84	9.42	9.94	-1.60	-2.28	-0.76	3322
19582 – 3833	-20.90	10.25	10.43	0.02	-2.26	-1.48	3332
20192 + 6634	-18.46	9.27	10.00	-0.86	-2.24	-1.72	3322
20243 – 0226	-20.55	10.11	10.41	-1.14	-0.27	-0.54	3332
20272 – 4738	-17.46	8.87	9.89	-2.01	-2.22	-0.74	3332
20338 + 5958	-19.59	9.72	9.11	-1.33	-2.37	-2.13	3322
20550 + 1655	11.60	-3.05	-1.96	0.44	3322
20551 – 4250	-21.49	10.48	11.73	-2.60	-2.17	0.49	3332
21008 – 4347	-19.23	9.58	10.76	-1.32	-2.50	-1.17	3332
21087 + 6557	-21.08	10.32	10.01	-1.00	-2.25	-1.45	3322
21171 – 0859	-18.96	9.47	9.90	-0.73	-2.41	-1.64	3332

Table 2—Continued

IRAS	M_B	$\text{Log}(L_B/L_\odot)$	$\text{Log}(L_{IR}/L_\odot)$	$\alpha(25,12)$	$\alpha(60,25)$	$\alpha(100,60)$	quality
21330 – 3846	-19.38	9.64	10.76	-1.56	-2.17	-0.82	3332
21457 – 8145	-20.72	10.18	9.95	-1.20	-2.35	-1.83	3332
23179 + 1657	-19.08	9.52	9.96	-0.78	-2.50	-1.26	3332
23192 – 4245	-20.09	9.92	9.43	-0.97	-2.30	-0.94	3332
23256 + 2315	-19.68	9.76	10.20	-1.53	-1.96	-0.78	3332
23336 + 0152	-20.07	9.91	10.35	-2.47	-1.47	-0.21	3232
23568 + 2028	-19.81	9.81	10.00	-0.74	-2.35	-1.31	3332

Table 3. Mean luminosities and ratios

Sample	N	$\log(\frac{L_E}{L_\odot})$	$\log(\frac{L_{IR}}{L_\odot})$	$\log(\frac{L_{IR}}{L_B})$
IRAS normal	185	9.9 ± 0.5	10.0 ± 0.5	0.12 ± 0.43
PDS starbursts	182	9.9 ± 0.4	10.3 ± 0.5	0.44 ± 0.48
PDS Sy1	31	10.3 ± 0.4	10.4 ± 0.7	0.13 ± 0.49
PDS Sy2	62	10.1 ± 0.5	10.4 ± 0.7	0.32 ± 0.49

Table 4. Spectral characteristics of the galaxies

IRAS	Other name	$\frac{[\text{OIII}]\lambda 5007}{\text{H}\beta}$	$\frac{[\text{NII}]\lambda 6584}{\text{H}\alpha}$	$\frac{[\text{SII}]\lambda(6717+6731)}{\text{H}\alpha}$	$\frac{[\text{OI}]\lambda 6300}{\text{H}\alpha}$	Activity Type
02395 + 3433	NGC1050	0.40	1.47	0.54	0.05	LINER
03419 + 6756	IC0342	0.08	0.43	0.24	0.01	SBNG
04435 + 1822	...	2.37	1.63	0.28	...	Sy2/LINER
07107 + 3521	...	4.10	0.60	0.31	0.04	Sy2
07278 – 6728	IC2202	11.72	0.60	1.21	...	Sy2
07568 + 1531	...	18.26	1.34	0.48	0.12	Sy2
08339 + 6517X	...	1.65	0.27	0.25	0.02	SBNG
10356 + 5345X	NGC3310	1.94	0.52	0.40	0.05	SBNG/LINER
11257 + 5850X – E	NGC3690	1.00	0.25	0.31	0.04	SBNG
11257 + 5850X – W	NGC3690	1.36	0.44	0.33	0.05	SBNG/LINER
12116 + 5448	MRK0201	1.13	0.47	0.26	0.03	SBNG
12398 – 0641	NGC4628	8.36	0.70	0.46	0.06	Sy2
12542 – 0815	NGC4818	0.14	0.65	0.19	0.01	SBNG/LINER
14454 – 4343	...	14.88	1.04	0.34	0.09	Sy2
19265 – 4338	...	6.48	1.02	0.72	0.20	Sy2
20243 – 0226	IIZw083	3.43	0.54	0.44	0.14	Sy2

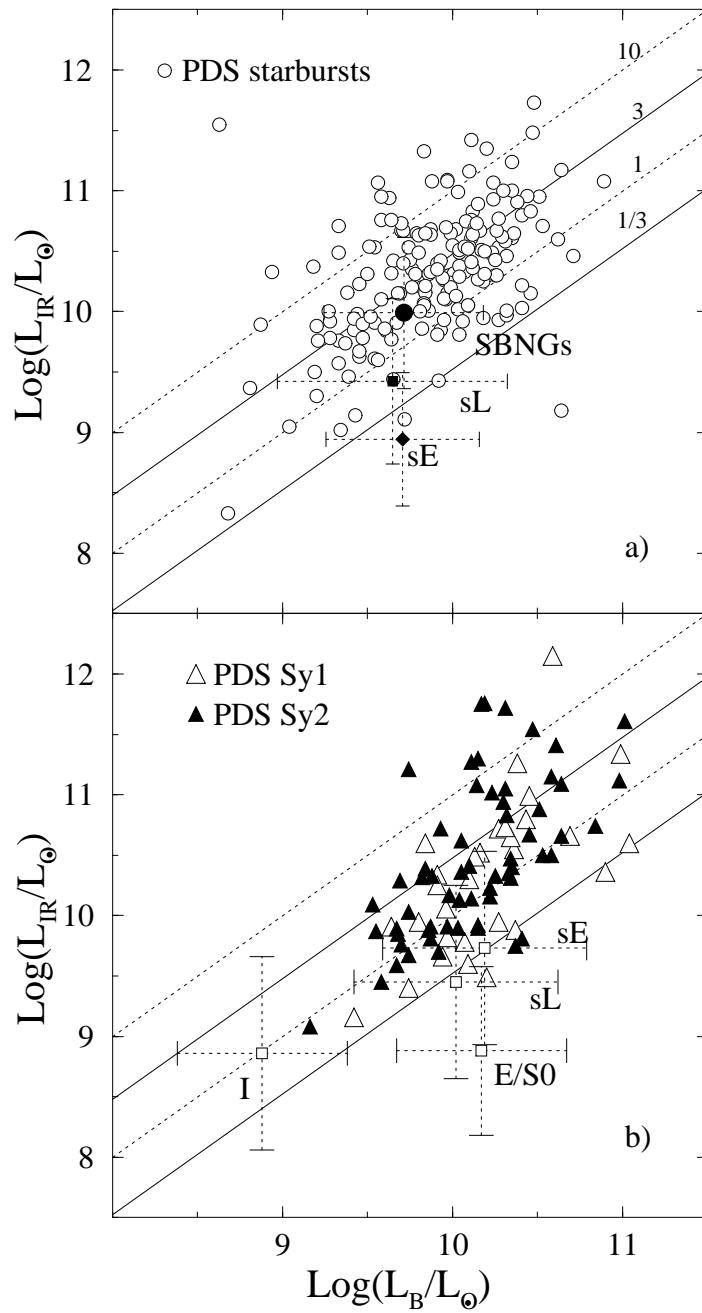


Fig.1

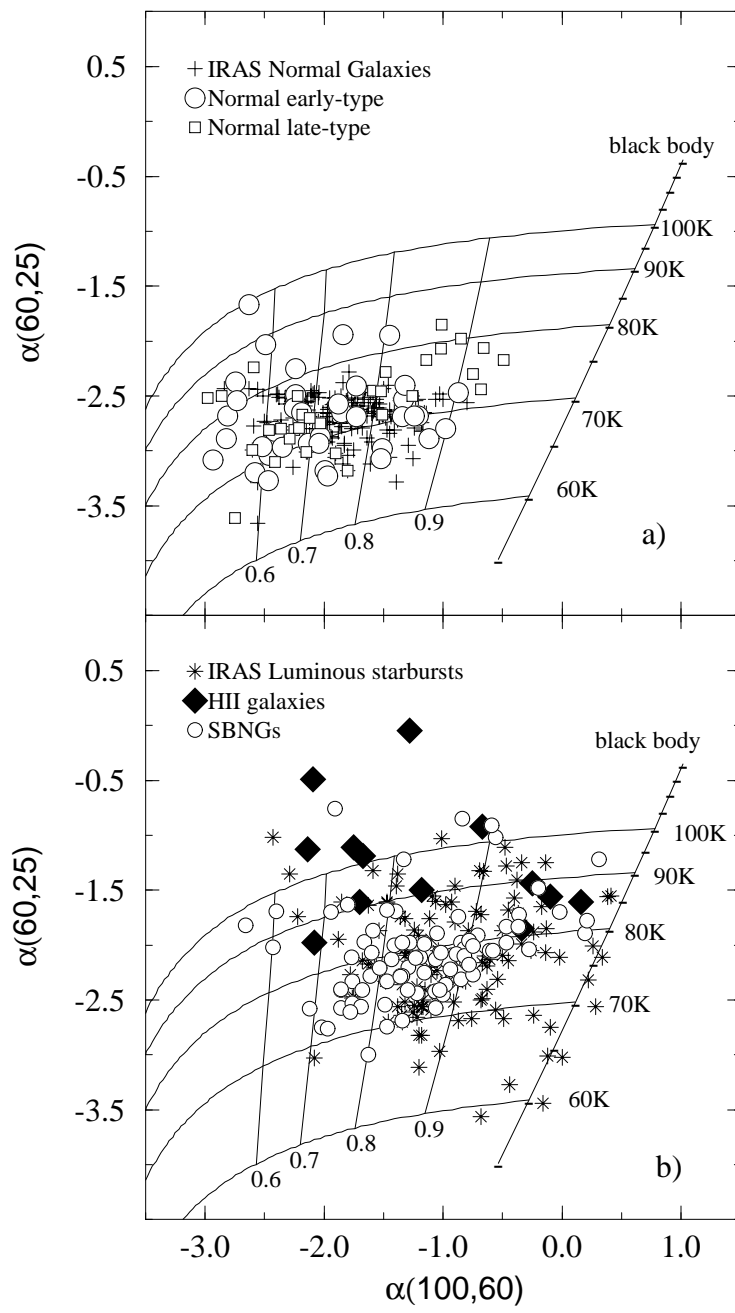


Fig. 2

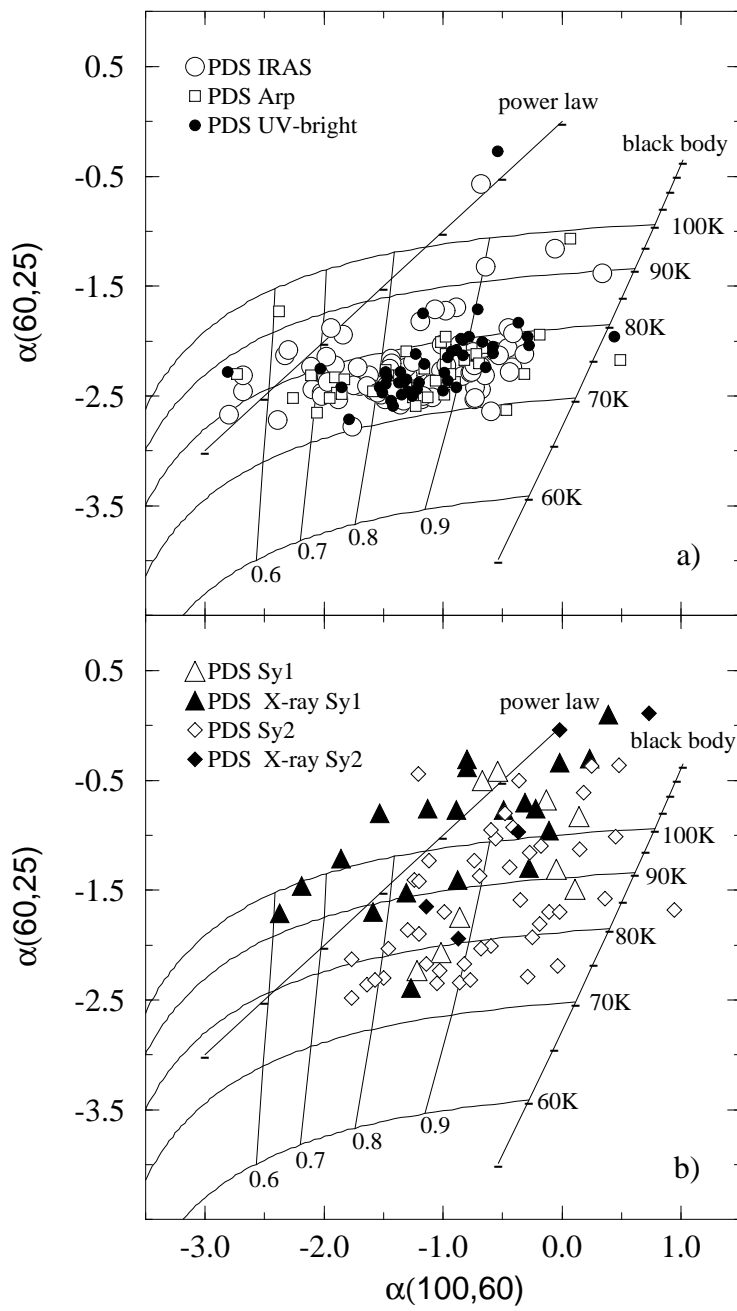


Fig. 3

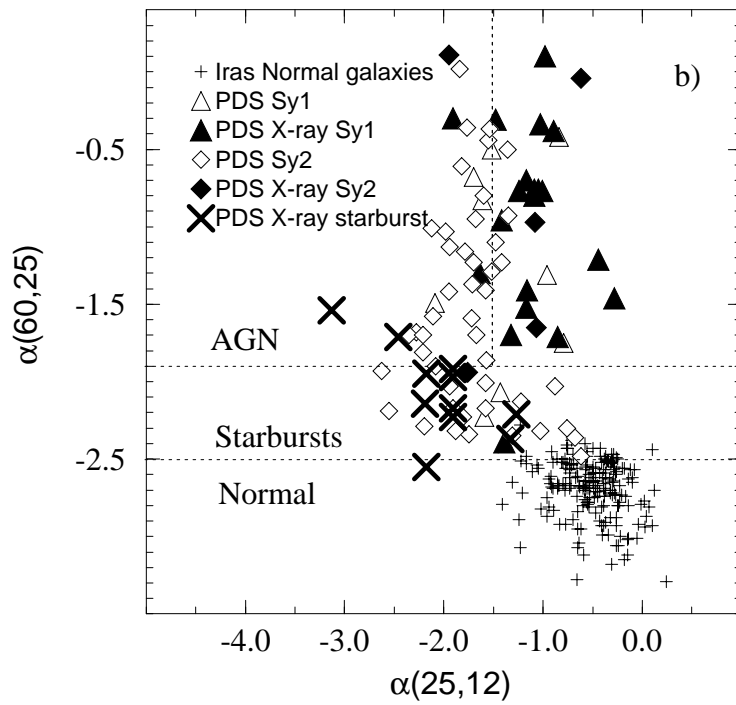
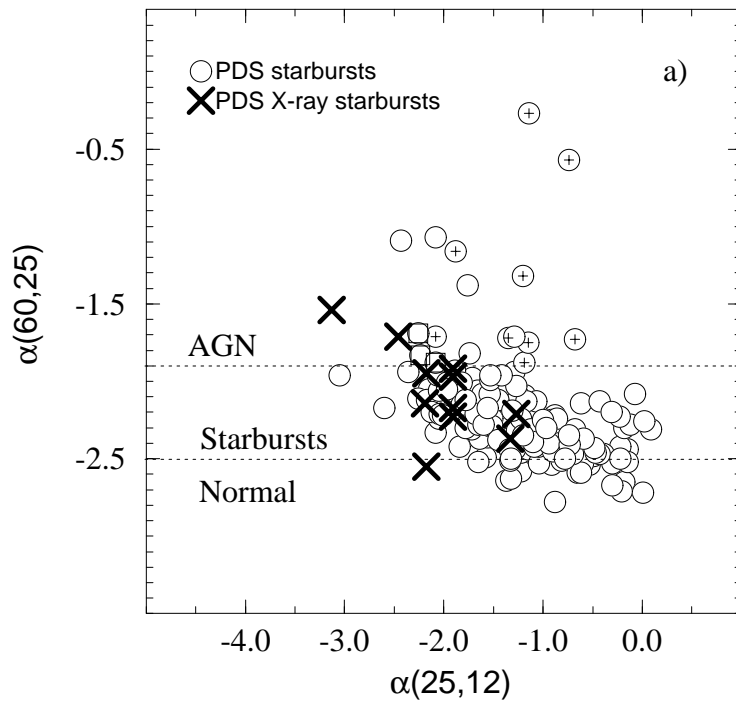


Fig. 4-

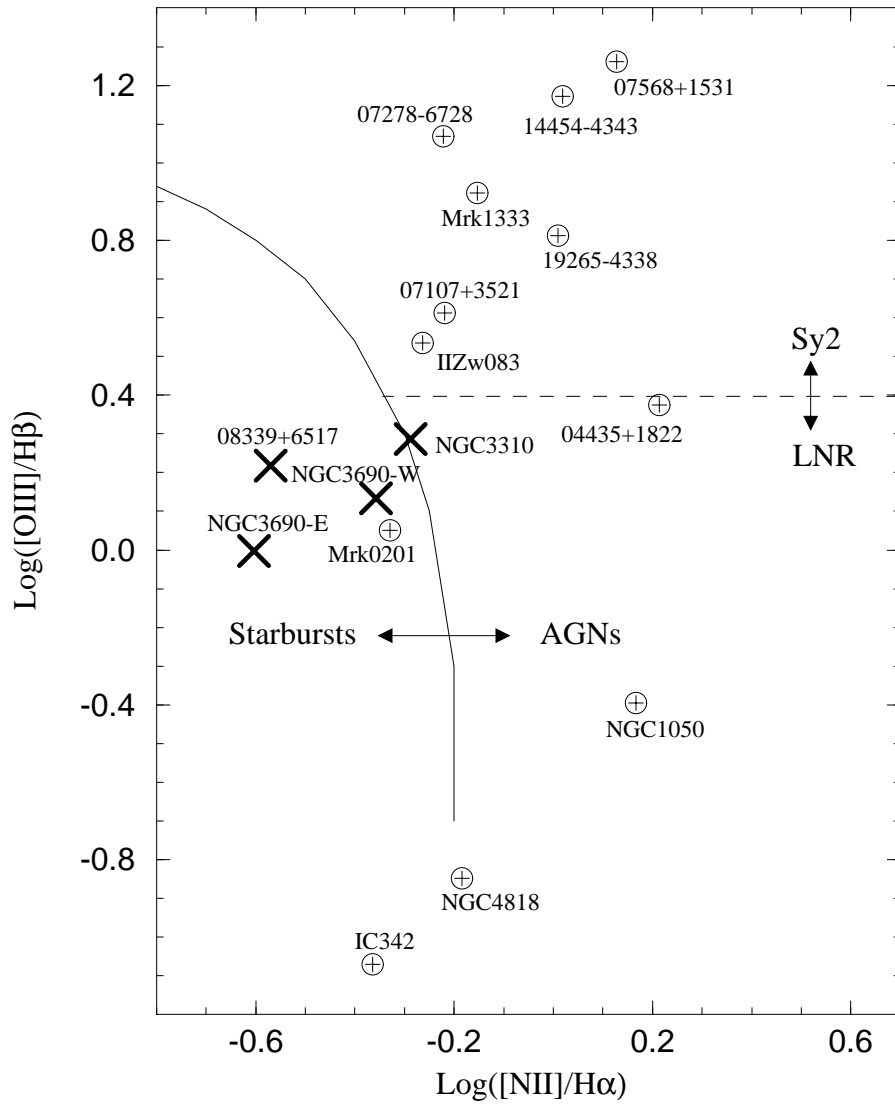


Fig. 5-

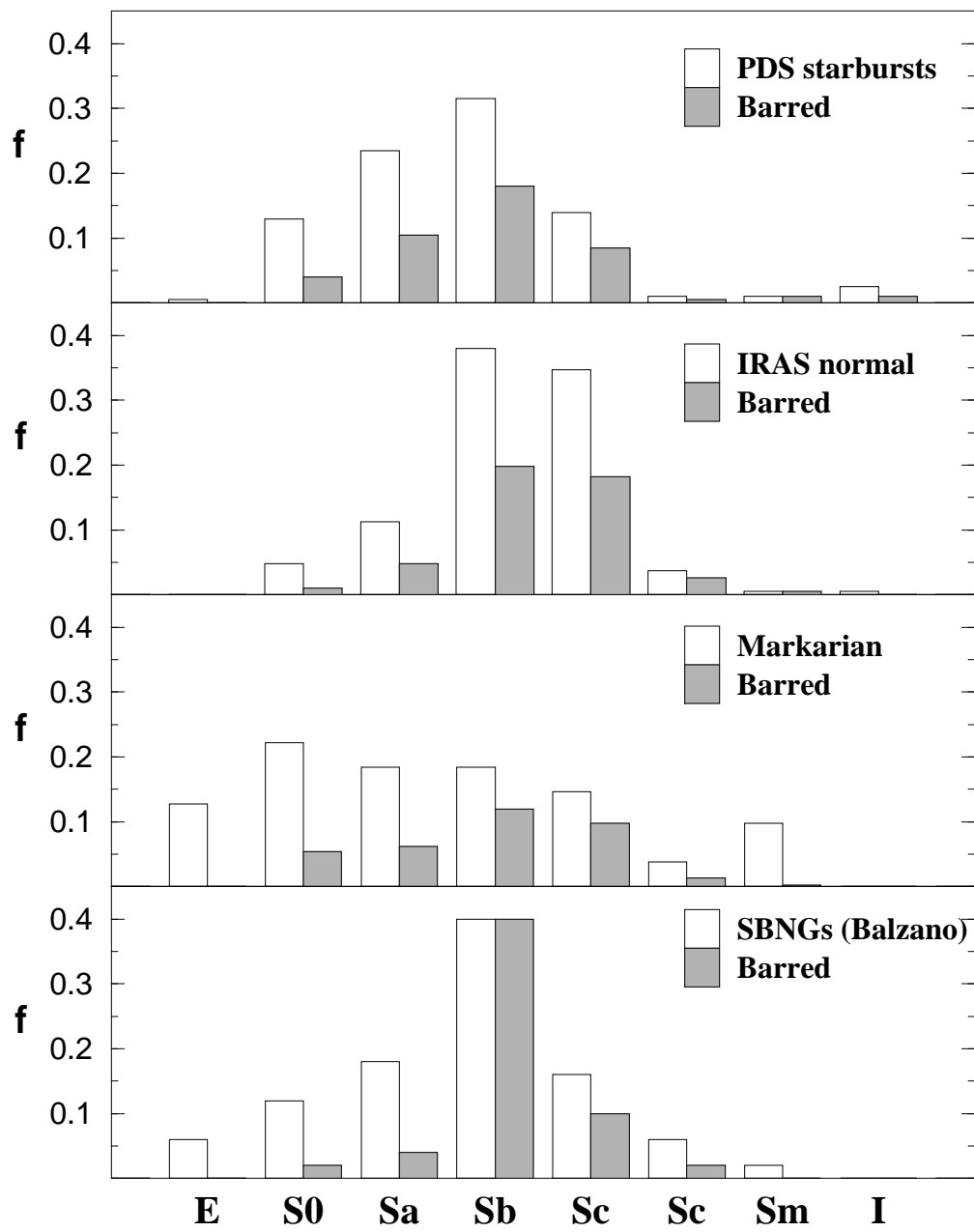


Fig. 6

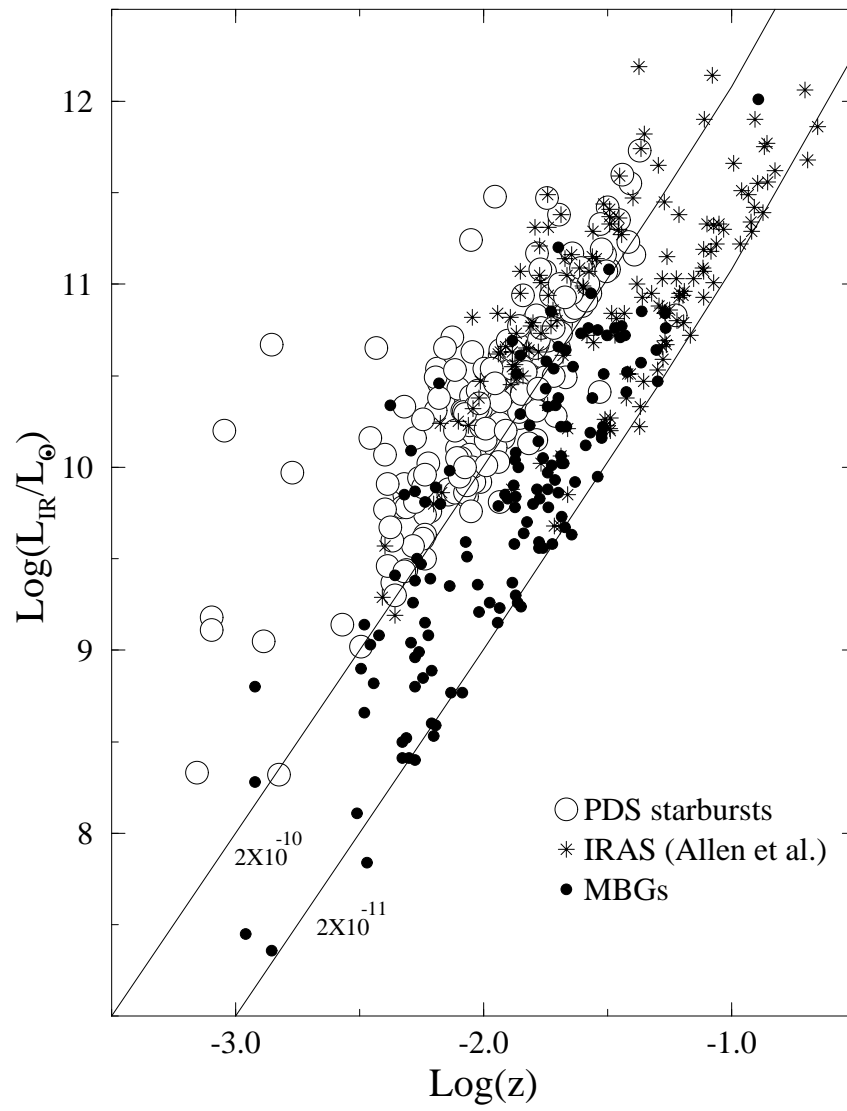


Fig. 7